Journal of
Composites Science

MDPI

Review

Thermal Effects and Glass Crystallization in Composite Matrices for Immobilization of the Rare-Earth Element–Minor Actinide Fraction of High-Level Radioactive Waste

Sergey V. Yudintsev [1], Michael I. Ojovan [1,2,*] and Victor I. Malkovsky [1]

[1] Institute of Geology of Ore Deposits, Petrography, Mineralogy, and Geochemistry of the Russian Academy of Sciences, Staromonetny Lane, 35, 119017 Moscow, Russia; yudintsevsv@gmail.com (S.V.Y.); malkovsky@inbox.ru (V.I.M.)
[2] Department of Materials, Imperial College London, London SW7 2AZ, UK
* Correspondence: m.ojovan@imperial.ac.uk

Abstract: The current policy of managing high-level waste (HLW) derived in the closed nuclear fuel cycle consists in their vitrification into B-Si or Al-P vitreous forms. These compounds have rather limited capacity with respect to the HLW (5–20 wt%), and their properties change over time due to devitrification of the glasses. Cardinal improvement in the management of HLW can be achieved by their separation onto groups of elements with similar properties, followed by their immobilization in robust waste forms (matrices) and emplacement in deep disposal facilities. One of the possible fractions contains trivalent rare-earth elements (REEs) and minor actinides (MAs = Am and Cm). REEs are the fission products of actinides, which are mainly represented by stable isotopes of elements from La to Gd as well as Y. This group also contains small amounts of short-lived radionuclides with half-lives ($T_{1/2}$) from 284 days (^{144}Ce) to 90 years (^{151}Sm), including ^{147}Pm ($T_{1/2}$ = 2.6 years), ^{154}Eu ($T_{1/2}$ = 8.8 years), and ^{155}Eu ($T_{1/2}$ = 5 years). However, the main long-term environmental hazard of the REE–MA fraction is associated with Am and Cm, with half-lives from 18 years (^{244}Cm) to 8500 years (^{245}Cm), and their daughter products: ^{237}Np ($T_{1/2} = 2.14 \times 10^6$ years), ^{239}Pu ($T_{1/2} = 2.41 \times 10^4$ years), ^{240}Pu ($T_{1/2}$ = 6537 years), and ^{242}Pu ($T_{1/2} = 3.76 \times 10^5$ years), which should be immobilized into a durable waste form that prevents their release into the environment. Due to the heat generated by decaying radionuclides, the temperature of matrices with an REE–MA fraction will be increased by hundreds of centigrade above ambient. This process can be utilized by selecting a vitreous waste form that will crystallize to form durable crystalline phases with long-lived radionuclides. We estimated the thermal effects in a potential REE–MA glass composite material based on the size of the block, the content of waste, the time of storage before immobilization and after disposal, and showed that it is possible to select the waste loading, size of blocks, and storage time so that the temperature of the matrix during the first decades will reach 500–700 °C, which corresponds to the optimal range of glass crystallization. As a result, a glass–ceramic composite will be produced that contains monazite ((REE,MA)PO_4) in phosphate glasses; britholite (Ca_x(REE,MA)$_{10-x}$(SiO_4)$_6O_2$) or zirconolite ((Ca,REE,MA)(Zr,REE,MA)(Ti,Al,Fe)$_2O_7$), in silicate systems. This possibility is confirmed by experimental data on the crystallization of glasses with REEs and actinides (Pu, Am). The prospect for the disposal of glasses with the REE–MA fraction in deep boreholes is briefly considered.

Keywords: nuclear waste; rare-earth elements; minor actinides; glass composite materials; monazite; zirconolite; britholite; thermal effects; borehole disposal

Citation: Yudintsev, S.V.; Ojovan, M.I.; Malkovsky, V.I. Thermal Effects and Glass Crystallization in Composite Matrices for Immobilization of the Rare-Earth Element–Minor Actinide Fraction of High-Level Radioactive Waste. *J. Compos. Sci.* **2024**, *8*, 70. https://doi.org/10.3390/jcs8020070

Academic Editor: Francesco Tornabene

Received: 17 December 2023
Revised: 31 January 2024
Accepted: 8 February 2024
Published: 10 February 2024

1. Introduction

For the third year in a row, the IAEA has revised the forecast for the growth of nuclear energy in the world [1]. It is now expected that in 2050, the nuclear power plant capacity will be 890 GW in the high version and 458 GW in the low version, up from the current value of 369 GW. Compared with the 2020 forecast, the upper limit is increased by 178 GW

(24%); compared with 2022, the high and low estimates increased by 2% and 14%. This correlates with estimates of economic growth, and additional impetus for nuclear energy development comes from concerns about climate change [2,3]. In November 2023, the European Parliament classified nuclear energy, along with 15 other technologies, as a "clean" technology, which will stimulate its further development. At the recent UN climate conference COP-28 in the UAE (30 November–12 December 2023), 22 countries, including the USA, Canada, France, Japan, the Republic of Korea, Sweden, and United Kingdom committed to increasing their nuclear power capacity in 2050 year 3-fold compared with 2020. Based on the growth in the capacity of nuclear power plants and under the condition of an open fuel cycle with the disposal of spent nuclear fuel (SNF), their operation will require 2–3 times more uranium than now; that is, from 130 to 200 thousand tons per year. This threatens the rapid depletion of available natural uranium resources if the basis of nuclear energy in the future continues to be only thermal neutron reactors—LWR, BWR, VVER [4].

Sustainable operation of nuclear energy will require (1) the provision of resources and (2) the development of methods for the effective and safe management of radioactive waste, including the most dangerous high-level radioactive waste (HLW) [5]. Both problems can be solved by the transition to a two-component nuclear power plant with slow and fast neutron reactors operating in a closed nuclear fuel cycle (NFC) mode with reprocessing of SNF [6]. This will allow fissile materials (U, Pu) to be involved in the NFC and creates the basis for the rational management of HLW by separating chemically similar elements into fractions that differ in half-lives, radiotoxicity, etc. One of these fractions consists of rare-earth elements (REEs) and minor actinides (Am, Cm), which can be co-extracted from HLW by improved PUREX, TRUEX, DIAMEX, UREX [7–15]. There are three known ways of solving the MA problem: (1) heterogeneous transmutation in fast neutron reactors after extracting the REEs and MAs, partitioning the MAs and REEs to separate Am and Cm; (2) combustion of MAs in molten salt reactors; (3) immobilization of the REE–MA fraction into stable matrices (waste forms) for disposal. Based on technological feasibility and efficiency, the third option for processing MAs by immobilization followed by disposal is the most preferable. Some glasses (La-borosilicate, LaBS), polyphase or monophase ceramics, and glass–crystalline composites with capacious and stable phases (artificial minerals), such as pyrochlore, zirconolite, britholite, brannerite, monazite, etc., are considered appropriate waste forms (matrices) of actinides.

Publications rarely consider the heating of matrices by radiogenic heat and its effect on the properties of materials. One of the consequences of radiogenic heating is the possibility of inducing spontaneous crystallization of the vitreous matrix (devitrification) and its transformation into a glass–ceramic. Here, we examine the available data on the content of REE—MA fractions in the SNF and HLW, their half-lives and radiogenic heat release during the decay, and the possibility of forming stable crystalline phases that immobilize MAs caused by the radiogenic heating of vitrified HLW.

2. REE and MA Contents in SNF and Reprocessing HLW

During the fission of actinides in a nuclear reactor, REEs are formed in large quantities; their share among fission products (FP) in the composition of spent fuel is about 30% [16,17]. The overwhelming majority of these elements are represented by stable isotopes or nuclides with such a long half-life that they can be considered stable (Table 1).

A small proportion of the REEs in SNF (HLW) are represented by short-lived isotopes (half-life $T_{1/2}$ up to 10 years: ^{144}Ce, ^{147}Pm, ^{154}Eu, ^{155}Eu) and medium-lived radionuclides ($T_{1/2}$ less than 100 years: ^{151}Sm). The decay of these REE radionuclides makes the main contribution to the heat released by SNF in the first few years after its removal from a nuclear reactor [18,19] (Tables 1 and 2, Figure 1).

Table 1. Isotopes of REEs and MAs in SNF, with a burnup 33 GW × d/t, after 3 years of storage [16,17].

Element	Total Content, g/t SNF	Radionuclide	Content, g/t	Half-Life, $T_{1/2}$
La	1205	-	-	Stable
Ce	2352	^{144}Ce	23	284 days
Pr	1109	-	-	Stable
Nd [1]	4000	-	-	Considered Stable
Pm	86	^{147}Pm	86	2.6 years
Sm [1]	777	^{151}Sm	16	93 years
Eu	133 g/t, including:	^{154}Eu	20	8.6 years
		^{155}Eu	12	4.8 years
Gd	76	-	-	Stable
Am	369 g/t, including:	^{241}Am	290	433 years
		^{243}Am	79	7370 years
Cm	20 g/t, including:	^{243}Cm	0.2	29 years
		^{244}Cm	18.3	18 years
		^{245}Cm	1.0	8500 years
		^{246}Cm	0.1	4760 years

[1] REEs with a very long half-life: ^{144}Nd (2.38×10^{15} years), ^{150}Nd (7×10^{18} years), ^{147}Sm (1.06×10^{11} years).

Table 2. The contribution of radionuclides to the heat released by spent fuel from a PWR reactor with a burn-up of 40 (a) and 60 (b) GW × d/t, in the range from 1 year to 500 years [18,19].

SNF Element Groups	Heat Release, W/t SNF, after 1–500 Years of SNF Storage							
	1	**10**	**30**	**50**	**70**	**100**	**300**	**500**
Cs/Sr/Ba/Rb	2765 [(a)]/ 4608 [(b)]	1054/ 1576	566/824	354/ 516	222/ 323	110/ 160	1/1	0
Ag/Pd/Ru/Rh	2752/3447	11/14	0	0	0	0	0	0
La/Ce/Pr/Nd/Pm/Sm/Eu	***3593/3843***	***64/109***	***10/17***	***2/3***	***0***	***0***	***0***	***0***
Np/Pu/Am/Cm/Bk	819/ 1515	348/ 785	332/ 613	309/ 516	287/ 449	258/ 381	159/ 199	116/ 139
Others	515/522	15/21	2/3	1/1	<0.1	<0.1	<0.1	<0.1
Total	**10,444/ 13,936**	**1492/ 2505**	**910/ 1458**	**666/ 1036**	**509/ 773**	**368/ 541**	**160/ 201**	**116/ 139**

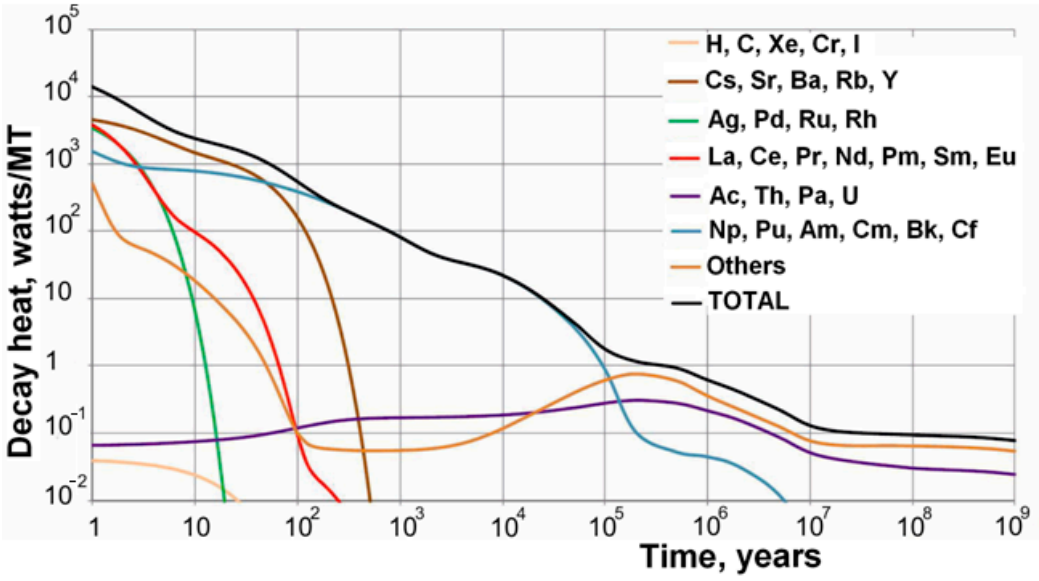

Figure 1. Contribution of decay of radionuclide groups to the heat released by spent fuel from a PWR reactor (burnup 60 GW × d/t) over 1 year to 10^9 years (see open access Refs. [18,19]).

Subsequently, the role of REEs quickly diminishes, and Cs, Sr, and trans-uranium actinides begin to play an increasingly important role (Table 2). After about 60 years, the contribution of the two groups of isotopes, Cs-Sr and actinides, will become equal; then, actinides will begin to make the main contribution to the heat released by SNF.

The ratio of the amounts of REEs and MAs (Am, Cm) in SNF is biased in favor of REEs; depending on the burnup of the fuel and its storage time, their content (Table 3) is 90–95 wt.% REE versus 10–5 wt.% of actinides (Am, Cm). The amount of ^{241}Am during SNF storage increases due to decay of the short-lived precursor ^{241}Pu. The heat released by the REE–MA fraction in accordance with its composition (Tables 1–5) is first determined by the decay of short-lived REEs, and then by ^{244}Cm, ^{241}Am, and, to a lesser extent, ^{243}Am.

Table 3. Content (a) in g/t of the main REE and actinide elements in SNF of light water reactors and their heat release (b) in W/t based on the fuel burn-up and storage time [10].

Element	After 5 Years of SNF Storage				After 30 Years of SNF Storage			
	45 GW × d/t		60 GW × d/t		45 GW × d/t		60 GW × d/t	
	(a)	(b)	(a)	(b)	(a)	(b)	(a)	(b)
Gd	150	0 (Stable)	310	0 (Stable)	180	0 (Stable)	346	0 (Stable)
Eu	190	60	260	90	170	8	230	12
Sm [1]	1060	0 (Stable)	1370	0 (Stable)	1120	0 (Stable)	1430	0 (Stable)
Pm	63	21	62	21	- [3]	-	-	-
Ce	3210	10	4230	10	3210	Stable	4220	Stable
Pr	1540	114	2010	113	1540	Stable	2010	Stable
Nd [2]	5570	Stable	7310	Stable	5570	Stable	7310	Stable
La	1670	Stable	2190	Stable	1670	Stable	2190	Stable
Σ REE	13,453	205	17,742	234	13,460	8	17,736	12
U	941,000	0.06	923,000	0.06	941,000	0.06	923,000	0.06
Pu	11,200	164	12,600	283	10,200	138	11,500	236
Np	570	0.01	780	0.02	570	0.01	780	0.02
Am	510	47	740	58	1380	146	1780	178
Cm	33	88	113	292	14	34	50	112
Am + Cm, MA	543	135	853	350	1394	180	1830	290
MA share [4]	4%	40%	5%	60%	9%	96%	9%	96%

[1] There is a long-lived ^{147}Sm ($T_{1/2}$ = 1.06 × 10^{11} years) and a small amount of ^{151}Sm ($T_{1/2}$ = 90 years). [2] Long-lived ^{144}Nd ($T_{1/2}$ = 2.4 × 10^{15} years) and ^{150}Nd ($T_{1/2}$ = 7 × 10^{18} years) can be considered stable. [3] absent. [4] It is the share of actinides in the REE–MA fraction and their contribution to heat release.

Table 4. Changes in the Am and Cm (MA) nuclide composition in SNF (burnup 45 GW × d/t) and their relative content in the hypothetical REE–MA fraction over storage time [20].

Nuclide, g/t SNF	After 1 Year	After 5 Years	After 30 Years
^{241}Am [1]	135	407	1272
^{243}Am	105	105	105
Total Am	240	512	1377
^{242}Cm	3.8	0.1	<0.01
^{244}Cm	35.3	30.3	11.6
^{245}Cm	2.2	2.2	2.2
Total Cm, including ^{243}Cm	41.9	33.0	14.4
Cm/(Am + Cm), %	15	6	1
MA/(REE + MA), %	2	4	9

[1] Content of ^{241}Am rises due to the decay of short-lived ^{241}Pu ($T_{½}$ = 14.4 years).

Table 5. Properties of Am and Cm in the SNF (burn-up 50 GW day/t) after 6 years of storage [21].

Radionuclide ($T_{1/2}$, Years)	Content, wt.%	Daughter Nuclide, ($T_{1/2}$, Years)	Type and Probability of Nuclides Decay	Heat Release, W/kg
^{241}Am (433)	63.8	^{237}Np (2.14×10^6)	α (≈1.0), SF [1] (3.77×10^{-12})	114.7
^{243}Am (7300)	25.4	^{239}Pu (2.41×10^4)	α (≈1.0), SF (3.7×10^{-11})	6.4
^{243}Cm (29)	0.1	^{239}Pu (2.41×10^4)	α (0.9976), β+ (0.0024)	1860.7
^{244}Cm (18)	9.8	^{240}Pu (6537)	α (≈1.0), SF (1.35×10^{-6})	2841.8
^{245}Cm (8500)	0.8	^{241}Pu (14.4)	α (1.0)	5.8
^{246}Cm (4760)	0.1	^{242}Pu (3.76×10^5)	α (≈1.0), SF (2.61×10^{-4})	10.2

[1] Spontaneous fission.

3. Effect of Radiogenic Heat on the Vitreous Matrix of the REE–MA Fraction

Stable elements or U and Th with a long half-life and low heat release are usually used in the laboratory synthesis and study of high-level waste matrices. For trivalent MAs (Am, Cm), REEs serve as simulants (Table 6); most often, Nd [22,23]. This approach is based on the proximity of the radii of Nd^{3+}, Am^{3+}, and Cm^{3+} [24]. It is justified when studying the solubility and isomorphic capacity of phases, the coordination of cations in the structure, and the distribution of elements between crystalline phases and glass.

Table 6. Examples of the use of elements—simulating radionuclides in HLW matrices.

Radionuclide	Radionuclide Simulants: From the More Similar to the Less Similar Elements				
	Short-Lived	Long-Lived	Stable Isotope of Element	Other Simulants	
Np	- [1]	U, ^{232}Th	Does not exist	Ce	Pr
^{238}Pu	-	U, ^{232}Th	Does not exist	Ce	Nd
^{239}Pu	^{238}Pu	U, ^{232}Th	Does not exist	Ce	Nd
Am, Cm	^{244}Cm	-	Does not exist	Nd	Sm
^{137}Cs	^{134}Cs	-	Natural isotopes (^{133}Cs, ^{127}I, ^{59}Co) or their mixtures ($^{86-88}$Sr, $^{90-96}$Zr)	Ba [2]	-
^{129}I	-	-		-	-
^{60}Co	-	-		-	-
^{90}Sr	-	-		Zr [2]	-
^{93}Zr	-	-		-	-
^{99}Tc	-	-	Does not exist	Re	Mo

[1] No data. [2] Simulants of decay products ^{137}Cs (^{137}Cs ⟶ ^{137}Ba) or ^{90}Sr (^{90}Sr ⟶ ^{90}Y ⟶ ^{90}Zr).

The similarity in the behavior of rare-earth elements (La, Nd) and MA (Am, Cm) in glass–crystalline matrices has been confirmed experimentally [25–27]. However, studies rarely consider the effect of the temperature factor—heating caused by the radiogenic heat. The use of high-capacity matrix compositions allows for a more efficient use of the space of future disposal facilities, which will reduce the specific costs of radioactive waste disposal. High short-lived radionuclide contents will cause heating of the matrix, which can change its properties. A few works [28–31] show that the temperatures of HLW matrices can reach several hundred degrees Celsius and persist for tens and hundreds of years. Due to the tendency of glass to crystallize at high temperatures, heating will have the greatest effect on vitreous matrices. If stable crystalline MA-containing phases are eventually formed, this will improve the immobilizing properties of the matrix. The phases comprise compounds of REEs and MAs with the structure of zirconolite, britholite, pyrochlore, brannerite, and monazite. The first four phases are characteristic of silicate glass–ceramics, and monazite appears during the crystallization of phosphate glasses. In essence, we are talking about the targeted crystallization of glass to obtain glass–ceramic compositions with increased stability. The idea of such transformations is considered in papers [32,33].

The advantages of glass–crystalline HLW matrices have been noted in many publications [32–39]. Considering the possible temperatures due to radiogenic heat, partial crystallization of glass with the formation of mineral-like phases of REEs and actinides

that are stable in water seems real. We have considered two scenarios for heating the vitreous matrix of REE and MA due to radiogenic heat: (1) for the REE–MA fraction, where REEs are considered to be stable elements; (2) for the REE fraction with the presence of radioactive isotopes. This makes it possible to estimate the temperatures of REE–MA matrices containing actinide and rare-earth radionuclides. Assessments of the heating of the matrix with rare-earth elements are of importance in connection with their possible release at SNF reprocessing, including the "dry" regeneration of SNF in molten salts [40–44] with subsequent immobilization of the so called "lanthanide fraction" in the glasses. This REE fraction of SNF reprocessing will have the following approximate composition (in wt.%): 38 Nd_2O_3, 24 CeO_2, 12 La_2O_3, 11 PrO_2, 8 Sm_2O_3, 5 Y_2O_3, 1 Eu_2O_3, and 1 Gd_2O_3. First, we will consider the change over time in the heat release and temperature of the matrix of the REE–MA fraction under the assumption that the REE isotopes are stable; then, we will carry out the calculation only for the REE fraction, taking into account short-lived radionuclides. The basics of the calculations are presented in [31].

4. Estimation of Temperature of the REE–MA Fraction Matrix When REEs Are Stable

The half-lives of ^{239}Pu and ^{237}Np are long (tens of thousands and millions of years), while short-lived ^{238}Pu (88 years) and ^{241}Pu (14 years) quickly decay to ^{234}U (246,000 years) and ^{241}Am (431 years), so Am and Cm become the main source of radiogenic heat in SNF, and they also determine the heat released by the REE–MA fraction. It is assumed that the REE–MA fraction contains 95 wt.% REE (stable) and 5 wt.% MA, including 3.5% ^{241}Am ($T_{1/2}$ = 432 years), 1% ^{243}Am (7370 years), 0.45% ^{244}Cm (18 years) and 0.05% ^{245}Cm (8500 years). Taking into account their heat release (W/kg)—^{241}Am, 114.7; ^{243}Am, 6.4; ^{244}Cm, 2841.8; ^{245}Cm—5.8 [21]—the initial heat released by the fraction can be attributed to two isotopes: ^{244}Cm (~78%) and ^{241}Am (~22%). It was assumed that the vitrified REE–MA fraction is loaded in a container with a diameter of 0.2 m and placed in a deep borehole in granites in the interval from 3 to 5 km; between the walls of the container with vitrified HLW and the borehole, there can be a layer of sorption bentonite buffer 10 cm thick or the buffer is absent. The parameters used in the calculations are summarized in Table 7.

Table 7. Thermophysical properties of the actinide matrix, sorption buffer, and host rocks [31,45].

Engineering Barrier Material, Waste-Hosting Rock	Density, kg/m^3	Specific Heat Capacity, J/(kg·K)	Thermal Conductivity, W/(m·K)
Glass with 30% REE-MA fraction	3000	900	1.1
Bentonite buffer layers	1700	1000	0.8
Granite, granite gneiss	2850	965	1.5

The changes over time in the intensity of the calculated heat released and temperatures in the center and on the surface of the block are shown in Figure 2. For the first few decades, their values change little, but then they quickly decrease following the decay of radioisotopes. Three years after loading the container into borehole, the temperatures in the center/on the surface of the block are 386/358 °C, and after 30 years, their values will be 201 and 190 °C. The presence of a bentonite buffer slightly increases the temperature (by 10 °C) due to its thermal conductivity being lower than that of the rock. To these values, it is necessary to add the increase in rock temperature due to the geothermal gradient, which, at a depth of 3–5 km, will be 100–150 °C. Thus, the temperature of a matrix with waste can reach 450–550 °C. An increase in the concentration of the REE-MA fraction in the glass or diameter of the block will cause its further increase.

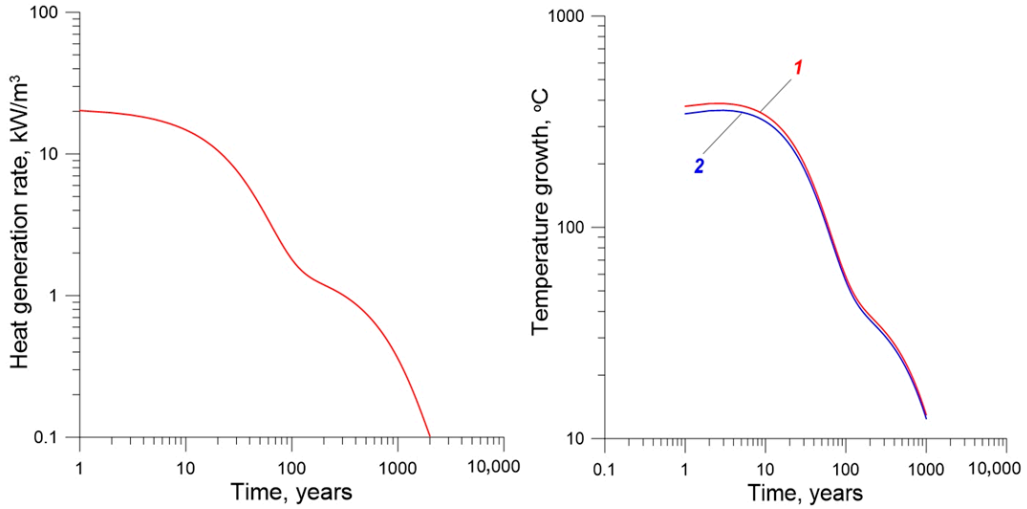

Figure 2. Time-dependence of heat release (**a**) and temperature (**b**) of a glass block with a diameter of 0.2 m with 30 wt.% REE-MA fraction (1—center; 2—surface). Spent fuel was stored for 1 year.

5. Temperature of the REE–MA Fraction Matrix with Decaying REE

SNF and HLW from reprocessing contain short-lived isotopes of rare-earth elements (Ce, Pm, Sm, and Eu). Therefore, it is necessary to evaluate the possible contribution of their decay to the heating of the REE waste form. In the first years after SNF is unloaded from the reactor, short-lived REEs make a significant contribution to heat release (Table 2, Figure 1) and then the Cs-Sr group begins to dominate; after 70 years, this role passes to trans-uranium elements. By analogy with calculations for the MA matrix, we estimated the temperature of glass containing the REE fraction. In the first years, the decay of short-lived radionuclides of this group will determine the heat release and heating of the SNF and the vitreous matrix of the HLW. Short-lived REE isotopes are represented by ^{151}Sm ($T_{1/2}$ = 90 years), which decays to ^{151}Eu (stable); ^{147}Pm (2.6 years) becomes ^{147}Sm (1.06×10^{11} years), then through α-decay, it transmutes into ^{143}Nd (stable); ^{144}Ce (284 days) → ^{144}Pr (17 min) → ^{144}Nd (stable); ^{154}Eu (8.8 years) → ^{154}Gd (stable); ^{155}Eu (5 years) → ^{155}Gd (stable). Taking into account the half-lives and contents of REE isotopes, the main contribution to the heat released by the REE mixture (Tables 1 and 2) will be made by ^{147}Pm and $^{154/155}$Eu. Let us assume that a tonne of SNF contains 15 kg of REEs (Table 3), which, during SNF reprocessing, enter liquid HLW and are then vitrified. With an REE concentration in glass equal to 30 wt.%, a tonne of vitreous matrix will contain 300 kg of REEs, and their amount in 1 m^3 (at a glass density of 3000 kg/m^3) will be 900 kg, which is 60 times higher than in a tonne of SNF. Taking this into account their heat release in SNF (Table 2), the change in the heat-release density of glass with 30 wt.% REE over time was determined as shown in Table 8. The very high volumetric heat release in the early years leads to extremely high temperatures of thousands of degrees Celsius (Figure 3). After 5–10 years of SNF storage, heat release due to the decay of short-lived REE radionuclides drops tens and hundreds of times (Table 8), so their contribution to matrix heating in 10 years will decrease to several tens of degrees.

Table 8. Dependence of the volumetric heat-release density of glass with 30 wt.% REE on time.

Storage Time, Years	1	5	10	30	50	70
Heat release, kW/m^3	216	12.3	3.8	0.6	0.1	0

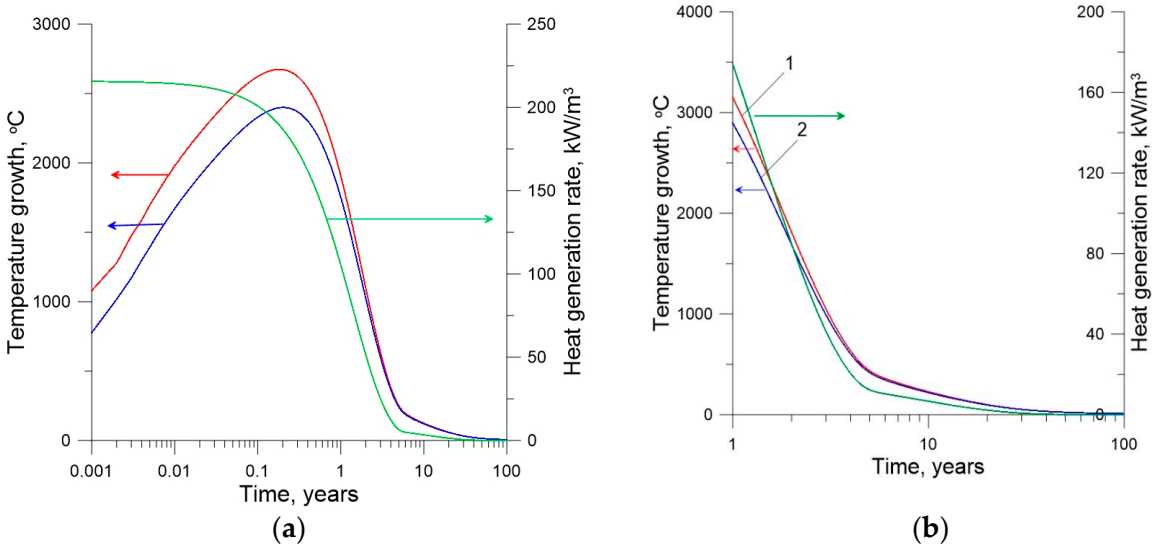

Figure 3. Heat release (green curve) and temperature of the glass matrix with 30 wt.% REE on the axis (1) and surface (2) of a block with a diameter of 0.2 m in the time interval from 0.001 year to 100 years (**a**) and from 1 year to 100 years (**b**). SNF was stored for 1 year before reprocessing.

The temperatures of a glass containing 50 wt.% REE from the pyrochemical processing of SNF were estimated [30]. Calculations were performed for a cylindrical block of glass with a diameter of 0.3–1.0 m; a residual amount of 0 to 20 rel.% of trans-uranium elements (TUEs) was allowed due to their incomplete extraction. The specific heat released by glass with a rare-earth element fraction depends on the degree of purification of this fraction from actinides and decreases with time. The heating temperature of a glass block increases with increasing diameter and TUE content but quickly decreases over time as REE isotopes decay (^{144}Ce, $T_{1/2}$ = 0.8 years; ^{147}Pm, 2.6 years; ^{151}Sm, 90 years; ^{154}Eu, 8.8 years; ^{155}Eu, 5 years). The initial temperature in the center of a block of glass with 50 wt.% REE varies from 200 to 900 °C, depending on the diameter (0.3–1 m) and the degree of purification from actinide content (80–100%), and quickly decreases after 3 years of storage.

6. General Patterns of Crystallization of Vitreous Matrices Containing HLW

Usage of glasses for the immobilization of HLW depends on two important parameters—the melting (T_m) and glass transition (T_g) temperatures, the latter being also known as the transition temperature at which the glass viscosity is 10^{13} Poise (10^{12} Pa/sec) [45–49]. The T_g value is determined by thermal analysis; it is not a constant value but weakly depends on the heating rate of the glass sample. The melting temperatures (T_m) of aluminum and iron phosphate glasses are 900–1000 °C, increasing to 1200–1300 °C for alkaline B-Si glasses and 1300–1500 °C for refractory aluminosilicate glasses. The ability of glass to crystallize depends on the rate of diffusion of elements and increases with decreasing viscosity. The maximum rate of devitrification occurs at temperatures 100–200 degrees above the glass transition temperature. To obtain large phase grains, heating is first carried out at 20–50 °C above T_g (Figure 4) to form crystallization centers (nucleation stage), and then the temperature is raised by 100–200 °C (growth stage of crystalline phases).

Heat-treatment schedules used to obtain a glass–ceramic are different for systems (A) with closely overlapping dependences of the nucleation and growth temperatures and those (B) with widely spaced temperatures of the maximum nucleation rate (I_{max}) and growth rate (U_{max}). For systems of type (B), only separate nucleation and growth of crystals is possible, whereas systems of type (A) can be processed by applying isothermal nucleation and growth or nucleation and growth under controlled cooling conditions [48,49].

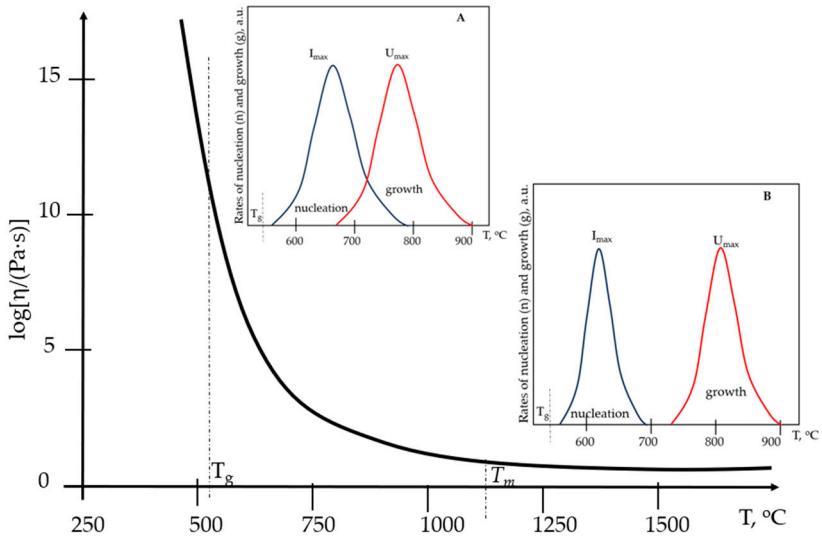

Figure 4. Change in glass viscosity with temperature (Pa × s); T_g—glass transition temperature. The insets show two types of the nucleation (I) and crystal growth (U) rates in arbitrary units [48,49].

Crystallization can begin after the melt is drained from the melter into the canisters due to residual heat [50,51]. Therefore, the cooling of the melt with HLW must be rapid in order to form a homogeneous glass. This is achieved by tempering it at a rate of 500 °C per hour, and when the glass cools at a rate of 50 °C per hour or less, crystalline phases appear [52]. The cooling rate is especially important near the glass transition temperature (T_g), below which the viscosity of the melt sharply increases, and it turns into glass. The T_g value depends on the composition of the glass and increases with melting temperature (T_m), amounting to 0.4–0.6 of the T_m value [53]. Heating accelerates devitrification due to a decrease in viscosity, which accelerates the diffusion of elements (Figure 4); this increases the number of crystallization centers and the rate of crystal growth. For Na-Al-P glasses (T_g being about 400 °C), the crystallization rate is maximum at ~500 °C; for Na-B-Si glasses (T_g ~550 °C), it is at 650 °C [35,45,52].

Typical T_g values for phosphate glasses with REE are in the range of 450–550 °C [53]. For B-Si glass matrices they increase to 550–600 °C; maximum values 650–790 °C, and even 870–900 °C, are typical of Al-Si glasses without boron [35,45,54–59]. The type of crystallization of glass during heating depends on the value of the $T_{gr} = T_g/T_m$ ratio; in the range of T_{gr} = 0.48–0.61, volumetric crystallization occurs, and at T_{gr} from 0.59 to 0.70, surface crystallization occurs [58]. An increase in T_g causes an increase in thermal stability of the glass matrix and, with it, the content of heat-generating radionuclides within it; an increase of 200 °C will allow for a 60% increase in the acceptable heat released by waste (e.g., concentration of short-lived isotopes) without crystallization of glass. Therefore, the waste loading of the Na-B-Si matrix is 3–5 times higher than that of Na-Al-P glass: 18–25 and 3–5 wt.%, respectively. Crystallization of glass is possible at temperatures lower than T_g, but due to its high viscosity, it will occur much more slowly. Depending on the position of the maximum rates of nucleation and crystallization on the temperature axis, the formation of glass–ceramics occurs during separate heating of the glass in several stages with a large difference in these temperatures (Figure 4) or in a single-stage process, where nucleation and the growth of crystals occur at the same temperature [48,49].

In industrial production, borosilicate glasses with HLW, after pouring the melt into a container containing several hundred kilograms of glass, cool naturally at a rate of about 1 °C/min [16]. Thus, for French B-Si glass R7T7 (T_g = 510 °C), the temperature drops to 400°C within 24 h after pouring the melt into canisters and then slowly decreases [37]. In order to avoid any risk of crystallization during storage and geological disposal, the temperature of the glass in the canisters (being increased due to radioactivity) must remain

below T_g so that the diffusion of atoms is negligible, which limits the amount of waste in the glass. Alternatively, this involves adapting its composition to increase the T_g of glass.

The choice of composition in the SiO_2–Al_2O_3–B_2O_3 system with the weight ratio SiO_2: Al_2O_3:B_2O_3 = 3:2:1 made it possible to include a 50 wt.% REE fraction—a mixture of La_2O_3, CeO_2, Nd_2O_3, Sm_2O_3, Gd_2O_3, Y_2O_3 or a simpler simulant (Nd_2O_3 + Gd_2O_3)—into homogeneous glass [30,42]. This increases the T_g value to 770–797 °C, which is significantly higher than the values for typical B-Si glass compositions for nuclear waste [35]. The melting point of such glasses, about 1450 °C, is also around 200–300 °C higher.

The heating of the matrix is influenced by its composition and radionuclide content, the dimensions of the container, and the thermophysical properties of the matrix and host rocks. It is possible to select the parameters at which the temperature within tens of years will be close to the glass transition temperature (T_g), which, for Al-P and B-Si glasses, varies from 500 to 700 °C [35,52]. As noted, in the manufacture of glass–ceramics, glass is heated in two stages: nucleation (1) and grain growth (2) at a higher temperature. The rate of formation of crystallization centers is maximum at a temperature slightly above T_g, and the highest rate of grain growth is 100–300 °C above T_g. This approach is used in experiments on the production of glass–ceramics; first, by heating the homogeneous glass at a temperature T = (T_g + 20–50 °C) and then increasing the temperature for crystal growth [48]. The duration of glass processing to obtain glass–ceramics ranges from 1–2 h to a few tens of hours. As a result, the glass turns into a glass–ceramic with double protection against leaching, since the stable crystalline phase with MAs is enclosed in glass with a lower actinide content. Heating of the matrix as a result of the decay of radionuclides will continue for decades, which will inevitably cause partial crystallization of the glass. Let us consider the experimental data on glass crystallization with simulants.

7. Experimental Studies of Crystallization of Glasses with REEs and Actinides

There are numerous works on the crystallization of glass matrices with HLW simulants to form glass–ceramics. Usually, in experiments, REEs, U, or Th are used to replace transuranium actinides (Np, Pu, Am, Cm). Crystallization products in silicate systems are represented by zirconolite ((Ca,Ln)(Zr,Ln)$(Ti,Al)_2O_{7)}$ or britholite ($(Ca,Ln)_{10}(SiO_4)_6O_2$), and when phosphate glass is heated, monazite $(Ca,Ln)PO_4$ is formed. The symbol Ln refers to individual REEs, primarily Nd, their mixtures, as well as the REE-MA fraction as a whole. These crystalline phases have long been studied as possible actinide matrices with the data on their radiation and corrosion resistance indicating promise for their use for this purpose [16,17,23,28,33,35,39,45,60–62]. The important thing is that they have natural analogues, including radioactive minerals containing REEs, U, and Th, with an age of many millions of years. Their study makes it possible to evaluate the behavior of matrices with similar artificial phases over very long time periods.

Crystallization of glasses with the formation of monazite, zirconolite, and britholite has been studied due to interest in them as potential matrices of REEs and MAs. Of greatest interest are those that provide information about the production conditions, properties of glasses, and their heat treatment modes, including composition and melting temperature, solubility of the REE, glass transition temperatures, composition of phases and glass, distribution coefficients of elements between them, corrosion resistance, etc.

7.1. Zirconolite Glass–Ceramics with REE

Data on silicate matrices with zirconolite are available from various studies [32,37,39,63–79]. In a two-stage synthesis, zirconolite glass–ceramics are obtained by melting a mixture of oxides at elevated temperatures, and then the glass is subjected to heat treatment (annealing) in one or more stages to crystallize the zirconolite [68–74]. When heating B-Si or Al-Si glasses containing REEs, depending on the composition, zirconolite or britholite appears; with a high content of Zr and REEs in the glass, both of these phases are present. Additions of B_2O_3, CaO, or Na_2O reduce the melting temperature of glass from 1400–1550 °C to 1200–1300 °C; as a result, the glass heating temperature for

the crystallization of zirconolite and britholite is also reduced to 600–800 °C [63,73]. An increase in the glass heating temperature promotes the growth of larger grains of crystalline phases with actinides.

Crystallization leads to a redistribution of elements between the glass and formed phases. The value of the distribution coefficient (K_p) for REEs (Ce, Nd, Gd) between zirconolite and glass varies from 1.5 to 3, increasing from light REEs to heavy rare-earth elements and yttrium [63–65,69–71]. The distribution coefficient (K_p) is defined as the ratio of concentrations of the element (radionuclide) in the crystalline phase to that in the vitreous phase at equilibrium. This explains the rather slight decrease in the element content in the residual glass as zirconolite crystallizes [75–79]. In general, the structure of zirconolite is preferable for the inclusion of heavy REEs of the yttrium group with a smaller ionic radius compared with larger cations of light REEs of the cerium group. Moreover, it is the latter that dominates in the composition of SNF and HLW and forms the basis of the REE-MA fraction (La, Ce, Nd). The solubility of REEs in typical Na-Al-B-Si glasses is estimated at 15–25 wt.%. By modifying the composition, this can be increased to 30 wt.% and even 40–50 wt.% [43]. TiO_2 and ZrO_2 are required for the formation of zirconolite so, in this case, the solubility of REEs in glass will be lower.

7.2. Britholite Glass–Ceramics

The maximum REE content in the zirconolite is 40 wt.% [23], and in the britholite, it reaches 75 wt.% [80]. Therefore, the REE content in glass–ceramics with britholite will also be approximately two times higher than in matrices with zirconolite. There are numerous examples of britholite crystallization from the melt or by quenching and annealing glass doped with lanthanides (Figure 5) and minor actinides (Am) [25–27,32,36,37,75,80,81].

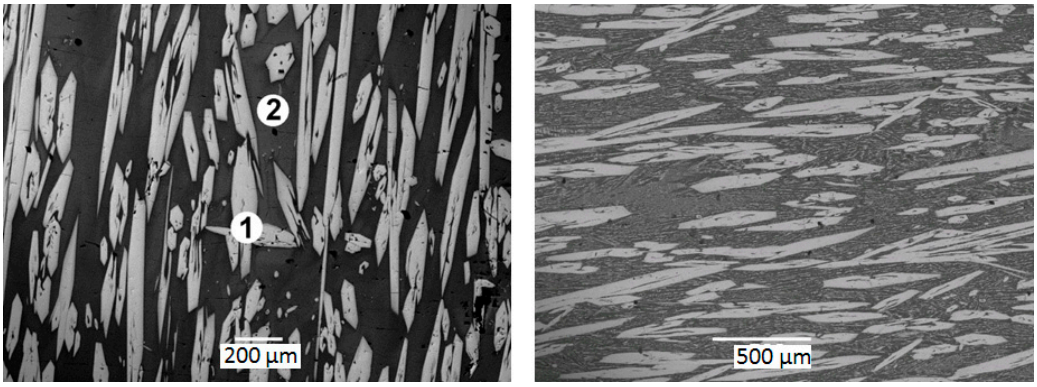

(**a**) (**b**)

Figure 5. SEM images of the glass–ceramics (**a**) with britholite (1) in residual glass (2), and (**b**) a sample after crystallization of the vitreous phase with britholite (light) in britholite–$CaSiO_3$ aggregates.

Distribution coefficient (K_p) values in the britholite–glass system for La, Ce, and Nd vary from 10 to 15 [80–82], while for Am, a K_p value of about 7–9 was established [25–27]. Considering the above, the residual glass of a glass–ceramic with britholite has a lower REE content than in glass–crystalline matrices with zirconolite. Since the stability of the glass phase is worse than that of the crystalline phases, this indicates a greater positive effect on the change in the immobilizing ability of the matrix in the case of britholite crystallization.

7.3. Monazite Glass–Ceramics

Phosphate glass–ceramics with monazite are described in [32,83–98]. Industrial immobilization of HLW in B-Si glass in the world has been carried out since the 1970s; in Russia, since the 1980s, an Al-P composition has been used for this purpose. To date, the total volume of vitrified waste can be estimated at 40,000 tons, including 32,000 tons of borosilicate glass and 8000 tons of phosphate glass [5]. Phosphate glasses are of interest from the

point of view of their easier transformation into a glass–ceramic matrix under radiogenic heating. Monazite glass–ceramics were obtained by melting an oxide–phosphate charge in alundum crucibles in an electric furnace at 1000 °C, followed by quenching and heating of the glass for 4 h in air at 500 °C. The calculated composition of sample AF-1 (wt.%) is as follows: 21.0% Na_2O, 17.0% Al_2O_3, 50.0% P_2O_5, 10.0% Ln_2O_3 (Ln = La + Ce + Nd), and 5.0% fission products (MoO_3, ZrO_2, BaO) and corrosion products (Cr_2O_3, Fe_2O_3, NiO, MnO). The samples are composed of glass and an REE phosphate with the structure of monazite (Figure 6), which is formed in the melt due to the excess of REE content over solubility, estimated at 2–3 wt.% [5,52,97,98].

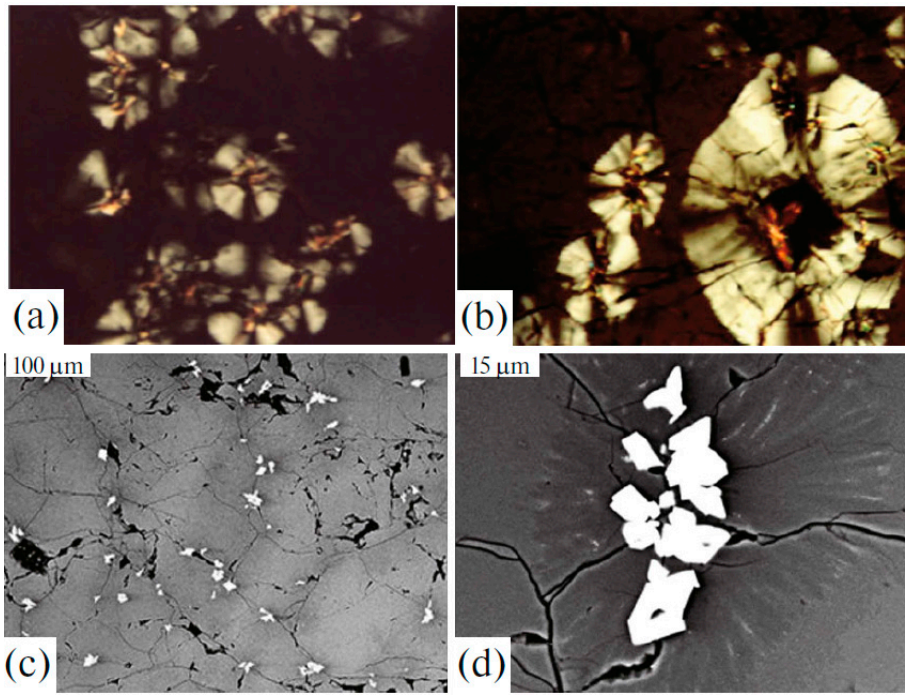

Figure 6. AF-1 glass after heating for 4 h at 500 °C. Images in an optical microscope, with crossed nicols, at a magnification of 60 (**a**) and 200 (**b**) (glass—dark; spherulites of Na-Al-P phases—light; monazite in the center—yellow). SEM images (**c**,**d**) of phosphate spherulites (dark gray) around monazite grains (white) in residual glass (light gray). Black—pores.

Monazite grains are up to 20 µm in size and form intergrowths. Partitioning of REEs is biased in favor of monazite, and the distribution coefficient (K_p) between monazite and glass is 30 (Table 9). Heating at 500 °C leads to the formation of Na-Al-P phases around the monazite grains (Figure 6 a,b). The spherulites practically do not contain any REEs.

Table 9. Composition (wt.%) of glass (1), monazite (2), and spherulites (3) in the AF-1 sample.

Phase	Na_2O	Al_2O_3	P_2O_5	Me^*O_{2-x}	SrO	ZrO_2	MoO_3	Cs_2O	BaO	$(Ln)^{**}{}_2O_3$
(1)	24.0	17.2	47.8	0.8	0.8	2.9	1.4	0.9	0.8	2.4
(2)	<d.l. [1]	<d.l.	27.9	<d.l.	0.5	<d.l.	<d.l.	0.6	0.3	72.1
(3)	25.5	19.1	51.3	1.4	<d.l	<d.l.	0.4	0.5	0.6	0.6

[1] Me*—Cr, Mn, Fe, Ni; Ln**—La, Ce, Nd; d.l—detection limit (0.3–0.5 wt.%).

Alumina phosphate (SAP) and alumina–iron phosphate (SAIP) glasses with REEs and actinides (U, Np, Pu, Am) have been studied [88,93–95]. Their compositions, in mol.%/wt.%, are as follows: 40/24.3 Na_2O, 20/20.0 Al_2O_3, 40/55.7 P_2O_5 (SAP); and 40/23.0 Na_2O, 10/9.5 Al_2O_3, 10/14.8 Fe_2O_3, 40/52.7 P_2O_5 (SAIP). The REE content varied

from 1 to 20 wt.%, and from less than 1 wt.% (Np, Pu, Am) to 50 wt.% (U) for actinides. The glass was obtained by melting for 0.5–6 h at 1000–1300 °C and pouring onto a plate for tempering or cooling according to a regime similar to cooling a block in a 200 L container at the "Mayak" Production Association. When the glass contains up to 5 wt.% REE, monazite does not form. When it is slowly cooled, phosphates of Na, Al (or Fe-Al), and REEs (monazite) appear, and the rate of the leaching of elements increases 5- to 10-fold to 10^{-6} g/(cm^2 × day) [93]. Actinide simulators (REEs) are concentrated in the monazite during crystallization; their distribution coefficient between monazite and residual glass is 45–70. The phase composition of glass matrices with REEs (La, Ce, Eu, Gd) and their structure and stability in water have been determined [94,95]. The introduction of up to 5 wt.% lanthanide oxides (Ln) into glasses does not cause crystallization during quenching (except for La-doped glass) and has a small effect on their structure and hydrolytic stability. At slow annealing, SAP glasses crystallize with the formation of Al-P, Na-Al-P, Ln-P (monazite), and Na-Ln-P phases, and additional oxide Gd_2O_3 in the case of Gd.

By melting for 1 to 6 h at 1000 or 1200 °C, alumina phosphate (SAP) and alumina–iron phosphate (SAIP) glasses with 9 wt.% REE were obtained. Part of the melt was quenched, and the rest was cooled in the furnace. Tempered glasses are homogeneous, while those cooled in a furnace, in addition to glass, contain Al, Na-Al, and rare-earth phosphate (monazite). Experiments (water; solid fraction 0.071–0.125 mm; 90 °C; 7 days) revealed an increase in the rate of leaching from partially crystallized glass of 5- to 10-fold compared with tempered glass. The inclusion of 9 wt.% REE does not impair the stability of glasses in water with respect to Na, Al, and P. For annealed glasses, leaching rates increase by 2–40-fold due to the formation of Al and Na-Al phosphates, but REE leaching remains low due to the occurrence of monazite. If glass crystallizes, monazite will retain REEs and prevent the properties of the matrix from deteriorating with time. Leaching rates on the 30th day are equal: 3.5 × 10^{-8}, 3.4 × 10^{-9}, and 6.3 × 10^{-9} g/(cm^2 × day) for Np, Pu, and Am, respectively. The higher leaching rates for Np than for Pu and Am are probably due to its presence, at least in part, as the NpO^{2+} ion [88].

According to [95], SAP (T_m = 1000 °C) and SAIP (T_m = 1200 °C) glasses with 10 wt.% REE do not contain crystalline phases, and only the sample with La contains traces of monazite ($LaPO_4$). When annealed, the REE-free SAP glass partially crystallizes, releasing $AlPO_4$ and β-$Na_6Al_3(P_2O_7)_3$. In glass with La_2O_3, the main phases are $AlPO_4$ and monazite. In the sample with Ce_2O_3, no crystalline phases other than $AlPO_4$ were found. The introduction of CeO_2 leads to the appearance of cerianite, monazite, and $Na_3Al_2(PO_4)_3$. Annealed samples with Pr and Nd oxides contain $AlPO_4$, monazite, and traces of $Na_3Al_2(PO_4)_3$. $Na_3REE(PO_4)_2$ orthophosphate was found in samples with Sm, Eu, and Gd. The content of REE oxides in the glass does not affect the leaching of Na, Al, Fe, or P. The REE leaching rates are 10^{-7}–10^{-6} g/(cm^2 × day). Tempered SAIP glasses are less soluble than SAP, and annealed samples are more stable than tempered ones due to the inclusion of REEs in monazite. After annealing, the yield of Na and P from SAP glass increases by 2- to 15-fold, but the leaching rates of Al, Fe, and REEs do not change.

Glass–ceramics containing up to 20 wt.% oxides (REEs) were obtained [94] by melting at 1250 °C and quenching or slow cooling to room temperature. Samples produced by heating SAP glass are composed of glass, $AlPO_4$, and monazite. Iron-containing glass–ceramics consist of glass, monazite, and Na-Al-Fe phosphate. Reducing the cooling rate of glass leads to the appearance of more crystalline phases. The leaching rates of Na, Al, Fe, and P are 10^{-5}–10^{-7} g/(cm^2 × day), and below 10^{-5} g/(cm^2 × day) for REEs.

The structure and properties of two Na-Al-(Fe)-P glasses with a 10 wt.% mixture of $(La_{0.57}Ce_{0.36}Nd_{0.93})O_3$ were studied [97]. Samples were prepared by melting for 1 h at 1200 °C and quenching. The solubility of REEs in glasses, in wt.%, are as follows: 0.8–0.9 La_2O_3, 0.7–0.8 CeO_2, 1.9–2.0 Nd_2O_3, for a total of 3.5 wt.%. The main proportion of REEs is found in monazite, which forms grains up to 10 microns in size. The K_p values between monazite and glass are equal to 17–20 (Ce), 17–21 (La), and 13–17 (Nd).

The possibility of producing a Fe-P glass–ceramic with monazite (Ce,La,Nd)PO_4 by melting–quenching was tested [91]. The mixture, loaded with up to 15 mol.% of REE imitator, was melted for 2 h at 1200 °C, and the melt was quenched into glass and annealed for 1 h at 450 °C to relieve stress. Differential thermal analysis was used to determine (Table 10) the glass transition temperatures (T_g), onset of crystallization (T_r), and melting temperatures (T_m). The T_g and T_r values firstly increase with an increase in the content of the actinide simulator (REE) and then decrease due to the formation of monazite (Ce,La,Nd)PO_4 followed by depletion of the residual glass in these elements. Thermal resistance of glass to crystallization correlates with the value of the ratio (T_r–T_g):(T_m–T_r); the higher it is, the more resistant the glass when heated. The resistance of glass to crystallization is also characterized by the ratio $\alpha = T_r/T_m$; at $\alpha \geq 0.6$, high thermal resistance is noted. The resulting glass–ceramics are resistant to corrosion, and their leaching rate in water is ~10^{-4} g m^{-2} day^{-1}. The optimal waste content in the matrix was determined to be 15 mol.% (22 wt.%).

Table 10. Values of T_g, T_r, T_L, $K_H = (T_r - T_g):(T_L - T_r)$, $\Delta T_{rg} = (T_r - T_g)$, $\alpha = T_r:T_g$ for the waste forms.

Samples	0 HLW	5 mol.% HLW	10 mol.% HLW	15 mol.% HLW
$T_g \pm 1$ (K)	778	790	773	770
$T_r \pm 1$ (K)	861	864	855	834
$T_L \pm 1$ (K)	1245	1246	1255	1264
ΔT_{rg} (K)	83	74	82	64
K_H	0.216	0.194	0.205	0.149
α	0.692	0.693	0.681	0.660

8. Synthesis of Glass–Ceramics by Heating a Mixture of Glass and Components of the Crystalline Phases

To obtain glass–ceramics, it has been proposed to sinter a mixture of glass, oxides of the crystalline phases, and waste at atmospheric [32,99,100] or elevated pressure, known as the hot-pressing method [45,49,101,102]. In this way, glass–ceramics with zirconolite (sintering for 0.5–1.5 h at 1000–1250 °C) and monazite were synthesized. In the second case, lanthanum metaphosphate glass was obtained by melting for 45 min at 1230 °C, which, after grinding, was pressed and sintered for 4 h at 1200 °C to obtain monazite glass–ceramics. In another variant, a mixture of HLW simulant and iron phosphate glass was pressed at a pressure of 30 MPa and sintered for 2–5 h at 500 °C to form glass–ceramics with monazite. As already noted, it is possible to select such contents of REE–MA waste fractions and block sizes so that, due to radiogenic heat, the temperature of the matrix is at 600–700 °C for several years. However, these methods require additional stages, which complicates the synthesis of highly radioactive materials and makes this process difficult to apply in the actual industrial production of these matrices.

Therefore, the main attention is paid to simpler methods of obtaining matrices by partial crystallization of the melt or by heating the tempered glass. This approach can use equipment that is already being used for the vitrification of HLW [90,91]. It is an optimal method for phosphate glass–ceramics with monazite due to its lower melting point compared with B-Si glasses.

9. Assessment of the Possibility for Deep-Borehole Disposal of REE–Actinide Matrices

The fight against climate change and energy geopolitics are leading to an increasing number of countries seeking to develop nuclear power. In this regard, the management of HLW is becoming increasingly urgent. In the coming years, it is planned to commission an SNF mine-type disposal facility in Finland, designed for 9000 tons of spent fuel.

However, long periods (30–50 or more years) from the start of searching for sites for a mine disposal facility to the start of its construction [103] make the alternative option of HLW disposal in deep boreholes attractive [104–111]. The first nuclear-waste storage

facility in deep boreholes can be created within five to ten years [105], which is an order of magnitude shorter than the construction time of traditional mine storage facilities.

Deep underground HLW disposal facilities can be of the mine type with a depth of about 0.5 km, in the form of vertical boreholes (3–5 km), or with their horizontal ending at a depth of 1–2 km. The advantages of placing waste packages in boreholes are noted for small-diameter containers with various HLW, including long-lived radionuclides. For deep-borehole disposal, waste forms with the following characteristics are preferred: low volume and package size, high specific activity, and/or high concentration of long-lived radionuclides, including fissile materials. In addition to better isolation due to a greater disposal depth than a shaft option, the borehole repository has the advantages of (i) cost efficiency; (ii) faster pre-operation, production and closure phases; and (iii) modularity. Of particular concern is the possibility of migration of long-lived actinides (Am, Pu, Np) in the form of colloids. Deep waters are Na-Ca brines with high ionic strength; this will cause colloids to aggregate into larger particles, settle out, and be retained by rocks, limiting the migration of radionuclides. In a deep-borehole repository, the temperature of the HLW matrix can reach significant values due to radiogenic heat and the natural thermal background of the host rocks due to the geothermal gradient.

The preferred types of HLW forms for placement into deep wells [108–115] are waste with high heat release, including chlorides and fluorides of Cs and Sr; cesium–strontium fractions; actinide-containing waste in a stable matrix, including Pu-containing waste; and the REE–actinide fraction of HLW. The advantages of the borehole disposal of HLW over mines include the following: long-term safety due to the large burial depth and extremely low solubility of actinides under reducing conditions; economical access to rocks with high insulating properties; lower infrastructure requirements and significantly smaller surface area; shorter terms of construction and placement of HLW; significantly lower cost; the possibility of creating waste in close proximity to the place of waste generation; extremely low probability of unauthorized access to radioactive materials; minimal control after HLW placement and storage-facility closure. In addition, the high salinity of the deep waters complicates the formation of a colloidal form of radionuclide transfer and the development of convection due to the heat released by HLW [115]. Field-research programs for deep-borehole disposal projects have been repeatedly discussed in the literature [111].

Promising matrices (waste forms) of REEs and MAs are considered to be the glasses of B-Al-Si, Ca-B-Al, Al-P, and Fe-P composition, as well as glass–ceramics with crystalline phases of zirconolite, britholite, and monazite [25–45,49,59,63–102,112–119]. The content of the REE-MA fraction in such matrices can reach 30–50 wt.%, and very deep wells with placement of the HLW forms at a depth of 3 to 5 km are optimal for their disposal.

10. Requirements for the Selection of HLW Matrices and Their Fractions

The nuclear waste forms must have certain properties and meet a number of criteria [46,61,112,120–126]; namely, high stability and tolerance to radiation effects, including transfer into new elements, ballistic effects, ion and electronic excitation, gas bubble and volumetric swelling effects, depending on the types of radionuclides; and a high waste loading (usually 20–35 wt.%) to reduce repository volumes. Waste forms must be chemically flexible and contain a mixture of radionuclides and associated waste elements. Matrices must be resistant to dissolution in water to minimize the release of radiotoxic substances, especially long-lived actinides. The manufacturing process must be simple and feasible using proven methods and without the use of vacuum or a special atmosphere. It is advisable to have natural mineral analogues in order to be confident in the reliability of the forecast of their long-term behavior. All these requirements are met by glass–ceramics with zirconolite, britholite, and monazite phases.

11. Use of Self-Heating of HLW for Deep Disposal

There are other proposals for using the heat of radioactive decay; for example, disposing highly radioactive waste by melting rocks and plunging them deep into the Earth's

core and even mantle [127–145]. The source of radiogenic heat capable of heating the surrounding rocks above 1200 °C may be spherical or cylindrical containers with a diameter of 0.1 m to 1 m containing actinides [137], HLW or SNF [138,139]; individual radioisotopes, for example 14 kg of ^{137}Cs or 0.5 kg ^{60}Co with a total activity of 3.85 × 10^{18} Bq [136]; or activity at the surface of 10^{17} Bq/m^2 [140]. The need to use containers made of a very refractory and expensive material (tungsten) is the least of the problems that arise with this approach. In another scenario, a container with HLW or SNF is placed into a pre-drilled hole filled with material with a lower melting point than the surrounding rocks [141–146], which facilitates their dipping. However, such proposals have not gone beyond theoretical calculations, which should also account for changes within the waste form [147,148].

12. Conclusions

The choice of glass–ceramics for the immobilization of HLW was proposed in the 1970s—20 years later than glass and ceramic forms [32,34,45,49]. Their formation occurs as a result of the controlled crystallization of a melt or glass in one or several stages. The distinction between uncontrolled (undesirable) and controlled (desirable) glass crystallization with an emphasis on HLW immobilization at high waste loadings has been reviewed [32]. To immobilize HLW, it is desirable to minimize the number of processing steps, so glass–ceramics are usually produced from a melt, where the nucleation and growth of crystals occur simultaneously during cooling or at an intermediate stage of exposure, rather than as a result of quenching the melt into glass and reheating it, as in the process of producing inactive commercial glass–ceramics. In the case of controlled nucleation and growth, the starting point is a single-phase melt or tempered glass, where crystals are formed by cooling from the melt or heating from the glass. If crystallization will occur upon cooling, it is important to design a system in which the nucleation and crystal-growth temperatures overlap. In another version of the synthesis, crystals are formed at high temperature—for example, during hot isostatic pressing (HIP) or high-temperature sintering—and its starting materials are usually solid mixtures of HLW powders and glass, or glass-forming oxides. The final product consists of crystalline phases embedded in intergranular glass, as demonstrated in glass–ceramics with U- or Pu-containing pyrochlore, apatite for wastes with high fluorine or chlorine content, and zirconolite with Pu. To obtain monazite glass–ceramics, glass powder from lanthanum metaphosphate is mixed with an HLW simulant (oxides of Nd, Zr, La, Ce, Fe, Mo) and heated to 1200 °C, then cooled in a switched-off furnace, obtaining monazite and the ZrP_2O_7 phase in the residual glass [84]. To suppress the formation of undesirable phases of ZrP_2O_7 or $FePO_4$, it was proposed to add B_2O_3 or TiO_2 in the initial batch [148–151].

To select the optimal regimes for glass–ceramic formation, data on melting, transition, and glass crystallization temperatures have great importance. For known HLW vitreous matrices, the glass transition temperatures range from 400 to 700 °C; the minimum values are characteristic of phosphate compositions, and the maximum values are typical of boron–aluminosilicate glasses. Since the growth of phase grains in glass begins when they are heated to 100–150 °C above the T_g, intensive crystallization of glass matrices with the formation of stable phases of radionuclides will occur in the range of 500–800 °C, which corresponds to the calculated temperatures under the influence of radiogenic heat. The heating was calculated for a matrix of the REE-MA fraction consisting of 95% REEs (all isotopes were considered stable) and 5% MAs, of which 3.5% was ^{241}Am ($T_{1/2}$ = 432 years), 1% was ^{243}Am (7370 years), 0.45% was ^{244}Cm (18 years), and 0.05 was ^{245}Cm (8500 years). Taking into account the heat released by isotopes (W/kg) is as follows: ^{241}Am—115, ^{243}Am—6, ^{244}Cm—2842, ^{245}Cm—6; the initial heat released by the matrix is mainly due to ^{244}Cm (~78%) and ^{241}Am (~22%). Although the bulk of REEs are found in SNF and HLW) as stable isotopes, some of them are radioactive with half-lives of 0.8–9 years (^{144}Ce, ^{147}Pm, ^{154,155}Eu) or 90 years (^{151}Sm). During the first few years, the contribution of REE decay to the heat released by SNF exceeds not only the share of heat release by actinides but also of such fission products as ^{90}Sr and ^{137}Cs. Over time, heat generation due to the decay

of REEs decreases, and after 10 years, it can be neglected. Therefore, the decay of REEs will affect the heating of the REE-MA matrix for a rather short time. When the matrix contains 30 wt.% of an REE-MA fraction, the temperature increase due to the decay of REEs in a year is estimated at 100 °C, and after 10 years, it will be less than 40 °C. Storing SNF before reprocessing will reduce the content and heat release by the shortest-lived isotopes of fission products, which include REEs and platinum-group metals. So, in 10 years, the heat released by SNF due to the decay of trans-uranium actinides and alkali and alkaline earth metals will decrease by 2- to 3-fold; for REEs, it will decrease by 50- to 60-fold, and for noble metals, by almost 300-fold. Before reprocessing, SNF is stored for 5–10 years and the effect of REE decay on the temperature can be neglected.

However, in the case of an ultra-deep borehole repository, it is necessary to take into account that the temperature at depths of 3–5 km increases by 90–150 °C due to the geothermal gradient. In combination with radiogenic heat, the temperature of the matrix with waste can be 500–800 °C for decades, which will cause crystallization of the glass with the appearance of stable phases of REEs and MAs—monazite in the phosphate system and zirconolite and britholite in the borosilicate system. The reality of this process is confirmed by data from numerous experiments on the partial crystallization of glasses with REEs and actinides. The distribution coefficients of REEs and actinides between crystals and residual glass are maximum for monazite in the phosphate system and britholite in silicate compositions and range from 10 to 30, which causes a decrease in their content in the residual glass during crystallization. The K_p of the elements between zirconolite and glass are an order of magnitude lower, so a significant part of the elements will be in the residual glass and, at exposure to water, can be leached from the glass–crystalline matrix.

Advantages of boreholes for high-level heat-generating waste disposal, including that of the REE-MA fraction, are as follows [106,110,115,121]: long-term safety due to the large depth of disposal; economical access to rocks with high insulating properties; low infrastructure requirements and small area of ground structures; short construction time, waste loading and sealing of the storage facility; the possibility of creating waste near the site of waste generation; low probability of unauthorized access; minimal control after the facility is closed; high water salinity, which prevents convection due to heat released by HLW; low solubility of actinides under reducing conditions; and instability of the colloids in brines.

Disadvantages and limitations associated with high temperatures include increased corrosion rates of the engineered barriers—the container, the bentonite buffer, and the matrix itself. It is critical to understand the thermodynamics and kinetics of phase separation and crystallization in HLW glasses in order to design glass–ceramics with the desired crystalline phase [49]. A major challenge in the design and development of waste glasses/glass–ceramics is their compositional complexity. In general, glass–ceramics with HLW include more than 30 different elements, including alkali, alkaline earth, multivalent transition and noble metals, as well as rare-earth elements and actinides, glass-forming oxides (Si, B, P, Al) (which complicates the nucleation and growth of various phases), and undissolved noble metals. TiO_2 and ZrO_2 in glass melts act as nucleating agents, so it is important to understand the distribution of elements in the crystalline phases, their size and morphology, as well as the chemistry of the residual glassy phase, in order to select and create durable glass–ceramic waste forms. Thus, traditional methods for studying the nucleation and growth from glasses may not be applicable to potentially heterogeneous industrial glass–ceramic systems that are produced in large ingots and thus cooled with different thermal profiles at different locations.

Due attention must be paid to the chemical resistance of glass–ceramics toward nuclear waste. Its stability in a geological repository is determined by the crystalline phases and chemical composition of the residual glass phase, as well as by the geochemical conditions of the surrounding rocks. Therefore, it is important to study the compositional dependence of crystallization behavior and its impact on the durability of the waste form. There is high interest in glass–ceramic forms of problematic waste with a high content of poorly soluble

components, such as heat-generating radionuclides, for waste from new types of nuclear reactors, as well as in the case of a higher waste load than traditional borosilicate glasses. For the immobilization of nuclear waste and the long-term thermal and chemical stability of HLW forms, crystallization can be useful, while the uniformity of structure during vitrification of HLW is considered a requirement for glassy materials [152–154]. Additional experiments and theoretical calculations are needed to test the possibility of crystallizing glass matrices under the influence of radiogenic heat and transforming them into stable glass–crystalline and crystalline forms of actinides, including the REE–MA fraction.

The concept of applying radiogenic heat to transform glass into glass–crystalline matrices has undeniable advantages over other approaches to immobilize actinide waste. One of the most important arguments in favor of this decision is the possibility of using well-developed routes for vitrification of the HLW using ceramic melters or inductively heated crucibles [16,32–41,45,48,49,80,81,95,116,126,155]. Both the technologies have been successively applied for many years at an industrial scale at radiochemical plants around the world [156–158].

Author Contributions: Conceptualization, S.V.Y.; methodology, S.V.Y.; formal analysis, S.V.Y., M.I.O. and V.I.M.; investigation, S.V.Y., M.I.O. and V.I.M.; resources, S.V.Y.; data curation, S.V.Y., M.I.O. and V.I.M.; writing—original draft preparation, S.V.Y.; writing—review and editing, S.V.Y., M.I.O. and V.I.M. All authors have read and agreed to the published version of the manuscript.

Funding: The study was carried out with financial support from the Ministry of Science and Higher Education of the Russian Federation within the framework of a state assignment for the Institute of Geology of Ore Deposits, Petrography, Mineralogy and Geochemistry of the Russian Academy of Sciences.

Data Availability Statement: All data is available within the manuscript.

Acknowledgments: The authors are grateful to the reviewers for comments and reviews.

Conflicts of Interest: The authors declare no conflicts of interest.

References

1. IAEA. *Energy, Electricity and Nuclear Power Estimates for the Period up to 2050*; International Atomic Energy Agency (IAEA): Vienna, Austria, 2023; 137p.
2. NEA. *Meeting Climate Change Targets. The Role of Nuclear Energy*; NEA No. 7628; OECD/NEA Publishing: Paris, France, 2022; 49p.
3. IEA. *Net Zero Roadmap: A Global Pathway to Keep the 1.5 °C Goal in Reach 2023 Update*; International Energy Agency: Paris, France, 2023; 224p.
4. NEA. *Transition towards a Sustainable Nuclear Fuel Cycle*; OECD/NEA Publishing: Paris, France, 2013; 67p.
5. Petrov, V.A.; Yudintsev, S.V. Mineral resources of the Russian nuclear industry and isolation of radioactive waste. *Geol. Ore Depos.* **2023**, *65*, 469–480. [CrossRef]
6. Adamov, E.O.; Asmolov, V.G.; Bolshov, L.A.; Ivanov, V.K. Two-component nuclear power. *Bull. Russ. Acad. Sci.* **2021**, *91*, 450–458. (In Russian)
7. IAEA. *Implications of Partitioning and Transmutation in Radioactive Waste Management*; Rep. 435; IAEA: Vienna, Austria, 2004; 126p.
8. Zilberman, B.Y.; Puzikov, E.A.; Ryabkov, D.V.; Makarychev-Mikhailov, M.N.; Shadrin, A.Y.; Fedorov, Y.S.; Simonenko, V.A. Development of a technological structure for processing irradiated nuclear fuel at npp using water extraction methods, its analysis and approaches to modeling. *At. Energy* **2009**, *107*, 273–284. (In Russian) [CrossRef]
9. Nash, K.L.; Lumetta, G.J. (Eds.) *Advanced Separation Techniques for Nuclear Fuel Reprocessing and Radioactive Waste Treatment*; Woodhead: Cambridge, UK, 2011; 492p.
10. NEA. *Spent Nuclear Fuel Reprocessing Flowsheet*; NEA OECD: Paris, France, 2012; 120p.
11. Modolo, G.; Geist, A.; Miguirditchian, M. Minor actinide separations in the reprocessing of spent nuclear fuels: Recent advances in Europe. In *Reprocessing and Recycling of Spent Nuclear Fuel*; Taylor, R., Ed.; Woodhead Publishing Series in Energy: Sawston, UK, 2015; Chapter 10; pp. 245–287.
12. Choppin, G.; Liljenzin, J.-O.; Rydberg, J.; Ekberg, C. The Nuclear Fuel Cycle. In *Radiochemistry and Nuclear Chemistry*, 4th ed.; Elsevier: Amsterdam, The Netherlands, 2013; Chapter 21; pp. 685–751.
13. Veliscek-Carolan, J. Separation of actinides from spent nuclear fuel: A review. *J. Hazard. Mater.* **2016**, *318*, 266–281. [CrossRef]
14. NEA. *State-of-the-Art Report on the Progress of Nuclear Fuel Cycle Chemistry*; OECD/NEA Publishing: Paris, France, 2018; 299p.

15. Baron, P.; Cornet, S.M.; Collins, E.D.; De Angelis, G.; Del Cul, G.; Fedorov, Y.; Glatz, J.P.; Ignatiev, V.; Inoue, T.; Khaperskaya, A.; et al. A review of separation processes proposed for advanced fuel cycles based on technology readiness level assessments. *Progr. Nucl. Energy* **2019**, *117*, 103091. [CrossRef]
16. Caurant, D.; Loiseau, P.; Majérus, O.; Aubin-Chevaldonnet, V.; Bardez, I.; Quintas, A. *Glasses, Glass-Ceramics and Ceramics for Immobilization of Highly Radioactive Nuclear Wastes*; Nova Science Publishers: New York, NY, USA, 2009; p. 445.
17. Ewing, R.C.; Weber, W.J. Actinide wasteforms and radiation effects. In *The Chemistry of the Actinide and Transactinide Elements*; Chapter 35; Morss, L.R., Edelstein, N.M., Fuger, J., Eds.; Springer: Dordrecht, The Netherlands, 2011; Volume 6, pp. 3813–3889.
18. Hardin, E.; Hadgu, T.; Clayton, D.; Howard, R.; Greenberg, H.; Blink, J.; Sharma, M.; Sutton, M.; Carter, J.; Dupont, M.; et al. Repository Reference Disposal Concepts and Thermal Load Management Analysis. FCRD-UFD-2012-00219. November 2012. Available online: https://www.energy.gov/ne/articles/repository-reference-disposal-concepts-and-thermal-load-management-analysis (accessed on 8 December 2023).
19. Carter, J.T.; Luptak, A.J.; Gastelum, J.; Stockman, C.; Miller, A. *Fuel Cycle Potential Waste Inventory for Disposition*; Savannah River National Laboratory: Aiken, SC, USA, 2012; 328p.
20. Collins, E.D.; Jubin, R.T.; DelCul, G.D.; Spencer, B.B.; Renier, J.P. Advanced Fuel Cycle Treatment, Recycling, and Disposal of Nuclear Waste. In Proceedings of the International Conference "Global 2009", Paris, France, 6–11 September 2009; pp. 2595–2602.
21. NEA. *Minor Actinide Burning in Thermal Reactors*; OECD/NEA Publishing: Paris, France, 2013; Report 6997; 78p.
22. Yudintsev, S.V.; Nickolsky, M.S.; Stefanovsky, O.I.; Nikonov, B.S. Crystal chemistry of titanates and zirconates of rare earths–possible matrices for actinide isolation. *Radiochemistry* **2022**, *64*, 667–679. [CrossRef]
23. Yudintsev, S.V.; Nickolsky, M.S.; Ojovan, M.I.; Stefanovsky, O.I.; Malkovsky, V.I.; Ulanova, A.S.; Blackburn, L.R. Zirconolite matrices for the immobilization of REE-Actinide wastes. *Ceramics* **2023**, *6*, 1573–1622. [CrossRef]
24. Shannon, R.D. Revised effective ionic radii and systematic studies of interatomic distances in halides and chalcogenides. *Acta Cryst.* **1976**, *A32*, 751–767. [CrossRef]
25. Kidari, A.; Magnin, M.; Caraballo, R.; Tribet, M.; Doreau, F.; Peuget, S.; Dussossoy, J.-L.; Bardez-Giboire, I.; Jégou, C. Solubility and partitioning of minor-actinides and lanthanides in alumino-borosilicate nuclear glass. *Procedia Chem.* **2012**, *7*, 554–558. [CrossRef]
26. Bardez-Giboire, I.; Kidari, A.; Magnin, M.; Dussossoy, J.-L.; Peuget, S.; Caraballo, R.; Tribet, M.; Doreau, F.; Jegou, C. Americium and trivalent Lanthanides incorporation in high-level waste glass-ceramics. *J. Nucl. Mater.* **2017**, *492*, 231–238. [CrossRef]
27. Tribet, M.; J'egou, C.; Miro, S.; Delrieu, J.; Doreau, F.; Peuget, S. Trivalent actinides and lanthanides incorporation and partitioning in UMo glass-ceramics. *J. Nucl. Mater.* **2023**, *585*, 154634. [CrossRef]
28. Ringwood, A.E.; Kesson, S.E.; Reeve, K.D.; Levins, D.M.; Ramm, E.J. Synroc. In *Radioactive Wasteforms for the Future*; Lutze, W., Ewing, R.C., Eds.; Elsevier: New York, NY, USA, 1988; Chapter 4; pp. 233–334.
29. Sizgek, G.D. Thermal consideration in a very deep borehole nuclear waste repository for Synroc. *Mat. Res. Soc. Symp. Proc.* **2001**, *663*, 2001. [CrossRef]
30. Choi, J.-H.; Eun, H.-C.; Lee, T.-K.; Lee, K.-R.; Han, S.-Y.; Jeon, M.-K.; Park, H.-S.; Ahn, D.-H. Estimation of centerline temperature of the wasteform for the rare earth waste generated from pyrochemical process. *J. Nucl. Mater.* **2017**, *483*, 82–89. [CrossRef]
31. Yudintsev, S.V.; Malkovsky, V.I.; Kalenova, M.Y. The thermal field around a borehole repository of radioactive waste. *Dokl. Earth Sci.* **2021**, *498*, 525–532. [CrossRef]
32. McCloy, J.S.; Schuller, S. Vitrification of wastes: From unwanted to controlled crystallization, a review. *Comptes Rendus. Géoscience* **2022**, *354* (Suppl. S1), 121–160. [CrossRef]
33. Ojovan, M.I.; Yudintsev, S.V. Glass, ceramic, and glass-crystalline matrices for HLW immobilisation. *Open Ceram.* **2023**, *14*, 100355. [CrossRef]
34. Hayward, P.J. Glass-ceramics. In *Radioactive Wasteforms for the Future*; Lutze, W., Ewing, R.C., Eds.; Elsevier: New York, NY, USA, 1988; Chapter 7; pp. 427–493.
35. Donald, I.W.; Metcalfe, B.L.; Taylor, R.N.J. The immobilization of high-level radioactive wastes using ceramics and glasses. *J. Mater. Sci.* **1997**, *32*, 5851–5887. [CrossRef]
36. Crum, J.; Maio, V.; McCloy, J.; Scott, C.; Riley, B.; Benefiel, B.; Vienna, J.; Archibald, K.; Rodriguez, C.; Rutledge, V.; et al. Cold crucible induction melter studies for making glass ceramic wasteforms: A feasibility assessment. *J. Nucl. Mater.* **2014**, *444*, 481–492. [CrossRef]
37. Caurant, D.; Majérus, O. Glasses and glass-ceramics for nuclear waste immobilization. In *Encyclopedia of Materials: Technical Ceramics and Glasses*; Pomeroy, M., Ed.; Elsevier: Oxford, UK, 2021; Volume 2, pp. 762–7904.
38. Ojovan, M.I.; Petrov, V.A.; Yudintsev, S.V. Glass crystalline materials as advanced nuclear wasteforms. *Sustainability* **2021**, *13*, 4117. [CrossRef]
39. Zhang, Y.; Kong, L.; Ionescu, M.; Gregg, D.J. Current advances on titanate glass-ceramic composite materials as wasteforms for actinide immobilization: A technical review. *J. Eur. Ceram. Soc.* **2022**, *42*, 1852–1876. [CrossRef]
40. Gombert, D.; Piet, S.; Trickel, T.; Carter, J.; Vienna, J.; Ebert, B. *Combined Waste form Cost Trade Study*; Contract DE-AC07-05ID14517; Idaho National Laboratory: Idaho Falls, ID, USA, 2008; 27p.
41. Gombert, D.; Ebert, W.; Marra, J.; Jubin, R.; Vienna, J. Global Nuclear Energy Partnership Waste Treatment Baseline. In Proceedings of the International Conference Atalante 2008, Montpellier, France, 19–22 May 2008.

42. Choi, J.-H.; Cho, I.-H.; Eun, H.-C.; Park, H.-S.; Cho, Y.-Z.; Lee, K.-R.; Park, G.-I.; Kim, S.-H.; Shin, C.-H.; Kim, J.-K. Fabrication and physical properties of lanthanide oxide glass wasteform for the immobilization of lanthanide oxide wastes generated from pyrochemical process. *J. Radioanal. Nucl. Chem.* **2014**, *299*, 1731–1738. [CrossRef]
43. Fadzil, S.M.; Hrma, P.; Schweiger, M.J.; Riley, B.J. Liquidus temperature and chemical durability of selected glasses to immobilize rare earth oxides waste. *J. Nucl. Mater.* **2015**, *465*, 657–663. [CrossRef]
44. Kashcheev, V.A.; Logunov, M.V.; Shadrin, A.Y.; Rykunova, A.A.; Schmidt, O.V. Strategy for the fractionation of HLW from SNF reprocessing. *Radioact. Waste* **2022**, *2*, 6–16. (In Russian) [CrossRef]
45. Donald, I.W. *Waste Immobilisation in Glass and Ceramic Based Hosts*; Wiley: Hoboken, NJ, USA, 2010; 507p.
46. Ojovan, M.I.; Lee, W.E.; Kalmykov, S.N. *An Introduction to Nuclear Waste Immobilisation*, 3rd ed.; Elsevier: Amsterdam, The Netherlands, 2019; 497p.
47. Zheng, Q.; Zhang, Y.; Montazerian, M.; Gulbiten, O.; Mauro, J.C.; Zanotto, E.D.; Yue, Y. Understanding glass through differential scanning calorimetry. *Chem. Rev.* **2019**, *119*, 7848–7939. [CrossRef] [PubMed]
48. Vernaz, E.; Gin, S.; Veyer, C. Waste glass. In *Comprehensive Nuclear Materials*; Konings, R., Allen, T., Stoller, R., Yamanaka, S., Eds.; Elsevier: Amsterdam, The Netherlands, 2012; Volume 5, pp. 451–483.
49. McCloy, J.S.; Goel, A. Glass-ceramics for nuclear-waste immobilization. *MRS Bull.* **2017**, *42*, 233–238. [CrossRef]
50. Stefanovsky, S.V.; Stefanovsky, O.I.; Remizov, M.B.; Kozlov, P.V.; Belanova, E.A.; Makarovsky, R.A.; Myasoedov, B.F. Sodium-aluminum-iron phosphate glasses as legacy high level wasteforms. *Progr. Nucl. Energy* **2017**, *94*, 229–234. [CrossRef]
51. Kozlov, P.V.; Remizov, M.B.; Belanova, E.A.; Vlasova, N.V.; Orlova, V.A.; Martynov, K.V. Modification of the composition of aluminophosphate glasses with HLW simulators to increase their stability. 1. The influence of modifiers on the viscosity and crystallization ability of melts. *Issues Radiat. Saf.* **2019**, *1*, 3–15. (In Russian)
52. Vashman, A.A.; Demine, A.V.; Krylova, N.V.; Kushnikov, V.V.; Matyunin, Y.I.; Poluektov, P.P.; Polyakov, A.S.; Teterin, E.G. *Phosphate Glasses with Radioactive Waste*; CNIIatominform: Moscow, Russia, 1997; 172p.
53. Musgraves, J.D.; Hu, J.; Calvez, L. (Eds.) *Handbook Springer of Glass*; Springer Nature: Cham, Switzerland, 2019.
54. Loiseau, P.; Caurant, D.; Majerus, O.; Baffier, N.; Fillet, C. Competition between internal and surface crystallization in glass-ceramics developed for actinides immobilization. *MRS Symp. Proc.* **2003**, *807*, 333–338. [CrossRef]
55. Litzkendorf, D.; Grimm, S.; Schuster, K.; Kobelke, J.; Schwuchow, A.; Ludwig, A.; Kirchhof, J.; Leich, M.; Jetschke, S.; Dellith, J.; et al. Study of lanthanum aluminum silicate glasses for passive and active optical fibers. Special Issue: Glass and Photonics—An Overview. *Appl. Glass Sci.* **2012**, *3*, 321–331. [CrossRef]
56. Lago, D.C.; Garcés, D.; Prado, M.O. Crystallization of an yttrium aluminosilicate glass for nuclear waste immobilization. *MRS Online Proc. Libr.* **2012**, *1475*, 227–232.
57. Moudir, D.; Souag, R.; Kamel, N.; Aouchiche, F.; Mouheb, Y.; Kamariz, S. Microwave chemical durability of an iron-rich glass-ceramic dedicated for high-level radioactive waste. *Mater. Res. Express* **2023**, *10*, 065503. [CrossRef]
58. Zanotto, E.D.; Tsuchida, J.E.; Schneider, J.F.; Eckert, H. Thirty-year quest for structure–nucleation relationships in oxide glasses. *Int. Mater. Rev.* **2015**, *60*, 376–391. [CrossRef]
59. Wu, L.; Li, H.; Wang, X.; Xiao, J.; Teng, Y.; Li, Y. Effects of Nd content on structure and chemical durability of zirconolite–barium borosilicate glass-ceramics. *J. Am. Ceram. Soc.* **2016**, *99*, 4093–4099. [CrossRef]
60. Guy, C.; Audubert, F.; Lartigue, J.-E.; Latrille, C.; Advocat, T.; Fillet, C. New conditionings for separated long-lived radionuclides. *C. R. Phys.* **2002**, *3*, 827–837. [CrossRef]
61. Lumpkin, G.R. Ceramic host phases for nuclear waste remediation. In *Experimental and Theoretical Approaches to Actinide Chemistry*, 1st ed.; Gibson, J.K., de Jong, W.A., Eds.; John Wiley & Sons Ltd.: Hoboken, NJ, USA, 2018; pp. 333–377.
62. Omel'yanenko, B.I.; Livshits, T.S.; Yudintsev, S.V.; Nikonov, B.S. Natural and artificial minerals as matrices for immobilization of actinides. *Geol. Ore Depos.* **2007**, *49*, 173–193. [CrossRef]
63. Loiseau, P.; Caurant, D.; Majerus, O. Crystallization study of (TiO_2, ZrO_2)-rich SiO_2-Al_2O_3-CaO glasses. Part I. Preparation and characterization of zirconolite-based glass-ceramics. *J. Mater. Sci.* **2003**, *38*, 843–852. [CrossRef]
64. Loiseau, P.; Caurant, D.; Majerus, O.; Baffier, N.; Fillet, C. Crystallization study of (TiO_2,ZrO_2)-rich SiO_2-Al_2O_3-CaO glasses. Part II. Surface and internal crystallization processes investigated by differential thermal analysis (DTA). *J. Mater. Sci.* **2003**, *38*, 853–864. [CrossRef]
65. Loiseau, P.; Caurant, D.; Baffier, N.; Mazerolles, L.; Fillet, C. Glass-ceramic nuclear wasteforms obtained from SiO_2–Al_2O_3–CaO–ZrO_2–TiO_2 glasses comtaining lanthanides (Ce, Nd, Eu, Gd, Yb) and actinides (Th): Study of internal crystallization. *J. Nucl. Mater.* **2004**, *335*, 14–32. [CrossRef]
66. Liao, C.-Z.; Liu, C.; Lee, P.-H.; Stennett, M.C.; Hyatt, N.C.; Shih, K. Combined quantitative X-ray diffraction, scanning electron microscopy, and transmission electron microscopy investigations of crystal evolution in CaO–Al_2O_3–SiO_2–TiO_2–ZrO_2–Nd_2O_3–Na_2O system. *Cryst. Growth Des.* **2017**, *17*, 1079–1087. [CrossRef]
67. Liao, C.-Z.; Liu, C.; Su, M.; Shih, K. Quantification of the partitioning ratio of minor actinide surrogates between zirconolite and glass in glass-ceramic for nuclear waste disposal. *Inorg. Chem.* **2017**, *56*, 9913–9921. [CrossRef] [PubMed]
68. Liao, C.-Z.; Shih, K.; Lee, W.E. Crystal structures of Al−Nd codoped zirconolite derived from glass matrix and powder sintering. *Inorg. Chem.* **2015**, *54*, 7353–7361. [CrossRef] [PubMed]

69. Loiseau, P.; Caurant, D. Glass–ceramic nuclear wasteforms obtained by crystallization of SiO_2–Al_2O_3–CaO–ZrO_2–TiO_2 glasses containing lanthanides (Ce, Nd, Eu, Gd, Yb) and actinides (Th): Study of the crystallization from the surface. *J. Nucl. Mater.* **2010**, *402*, 38–54. [CrossRef]
70. Martin, C.; Ribet, I.; Frugier, P.; Gin, S. Alteration kinetics of the glass-ceramic zirconolite and role of the alteration film–comparison with the SON68 glass. *J. Nucl. Mater.* **2007**, *366*, 277–287. [CrossRef]
71. Caurant, D.; Bardez, I.; Loiseau, P. Crystallization of $CaHf_{1-x}Zr_xTi_2O_7$ ($0 < x < 1$) zirconolite in SiO_2–Al_2O_3–CaO–Na_2O–TiO_2–HfO_2–ZrO_2–Nd_2O_3 glasses. *J. Mater. Sci.* **2007**, *42*, 10203–10218.
72. Caurant, D.; Loiseau, P.; Bardez, I.; Gervais, C. Effect of Al_2O_3 concentration on zirconolite ($Ca(Zr,Hf)Ti_2O_7$) crystallization in (TiO_2,ZrO_2,HfO_2)-rich SiO_2–Al_2O_3–CaO–Na_2O glasses. *J. Mater. Sci.* **2007**, *42*, 8558–8570. [CrossRef]
73. Caurant, D.; Majerus, O.; Loiseau, P.; Bardez, I.; Baffier, N.; Dussossoy, J.L. Crystallization of neodymium-rich phases in silicate glasses developed for nuclear waste immobilization. *J. Nucl. Mater.* **2006**, *354*, 143–162. [CrossRef]
74. Xu, H.; Wang, Y. Crystallization sequence and microstructure evolution of Synroc samples crystallized from $CaZrTi_2O_7$ melts. *J. Nucl. Mater.* **2000**, *279*, 100–106. [CrossRef]
75. Chouard, N.; Caurant, D.; Majerus, O.; Guezi-Hasni, N.; Dussossoy, J.-L.; Baddour-Hadjean, R.; Pereira-Ramos, J.-P. Thermal stability of SiO_2–B_2O_3–Al_2O_3–Na_2O–CaO glasses with high Nd_2O_3 and MoO_3 concentrations. *J. Alloys Compd.* **2016**, *671*, 84–99. [CrossRef]
76. Loiseau, P.; Caurant, D.; Baffier, N.; Fillet, C. Neodymium incorporation in zirconolite-based glass-ceramics. *Mater. Res. Soc. Symp. Proc.* **2001**, *663*, 169–178. [CrossRef]
77. Loiseau, P.; Caurant, D.; Baffier, N.; Mazerolles, L.; Fillet, C. Development of zirconolite-based glass-ceramics for the conditioning of actinides. *Mater. Res. Soc. Symp. Proc.* **2001**, *663*, 179–188. [CrossRef]
78. McGlinn, P.J.; Advocat, T.; Loi, E.; Leturcq, G.; Mestre, J.P. Nd- and Ce-doped ceramic-glass composites: Chemical durability under aqueous conditions and surface alteration in a moist clay medium at 90 °C. *Mater. Res. Soc. Symp. Proc.* **2001**, *663*, 249–258. [CrossRef]
79. Advocat, T.; McGlinn, P.J.; Fillet, C.; Leturcq, G.; Schuller, S.; Bonnetier, A.; Hart, K. Melted synthetic zirconolite-based matrices: Effect of cooling rate and heat treatment on ceramic microstructure and chemical durability. *Mater. Res. Soc. Symp. Proc.* **2001**, *663*, 277–284. [CrossRef]
80. Yudintsev, S.V.; Stefanovsky, S.V.; Kalenova, M.Y.; Nikonov, B.S.; Nikolsky, M.S.; Ananyev, A.V.; Shchepin, A.S. Matrices for the immobilization of rare earth-actinide fraction waste, obtained by induction melting in a cold crucible. *Radiochemistry* **2015**, *57*, 321–333. [CrossRef]
81. Smelova, T.V.; Krylova, N.V.; Yudintsev, S.V.; Nikonov, B.S. Silicate Matrix of Actinide-Bearing Wastes. *Dokl. Earth Sci.* **2000**, *374*, 149–1152.
82. Kim, M.; Heo, J. Calcium-borosilicate glass-ceramics wasteforms to immobilize rare-earth oxide wastes from pyro-processing. *J. Nucl. Mater.* **2015**, *467*, 224–228. [CrossRef]
83. Day, D.E.; Wu, Z.; Ray, C.S.; Hrma, P. Chemically durable iron phosphate glass wasteforms. *J. Non-Cryst. Solids* **1998**, *241*, 1–12. [CrossRef]
84. He, Y.; Lü, Y.; Zhang, Q. Characterization of monazite glass–ceramics as wasteform for simulated α-HLLW. *J. Nucl. Mater.* **2008**, *376*, 201–206. [CrossRef]
85. Li, H.; Liang, X.; Wang, C.; Yu, H.; Li, Z.; Yang, S. Influence of rare earth addition on the thermal and structural stability of CaO-Fe_2O_3-P_2O_5 glasses. *J. Mol. Struct.* **2014**, *1076*, 592–599. [CrossRef]
86. Wang, F.; Liao, Q.; Dai, Y.; Zhu, H. Properties and vibrational spectra of iron borophosphate glasses / glass-ceramics containing lanthanum. *Mater. Chem. Phys.* **2015**, *166*, 215–222. [CrossRef]
87. Wang, F.; Liao, Q.; Dai, Y.; Zhu, H. Immobilization of gadolinium in iron borophosphate glasses and iron borophosphate based glass-ceramics: Implications for the immobilization of plutonium. *J. Nucl. Mater.* **2016**, *477*, 50–58. [CrossRef]
88. Danilov, S.S.; Stefanovsky, S.V.; Stefanovskaya, O.I.; Vinokurov, S.E.; Myasoedov, B.F.; Teterin Yu, A. Aluminum (iron) phosphate glasses containing rare earth and transuranium elements: Phase composition, oxidation state of Np and Pu, and hydrolytic durability. *Radiochemistry* **2018**, *60*, 434–439. [CrossRef]
89. Wang, Y.; Wang, F.; Wang, Q.; Zhu, H.; Xiang, G.; Liao, Q.; Zhu, Y. Effect of neodymium on the glass formation, dissolution rate and crystallization kinetic of borophosphate glasses containing iron. *J. Non-Cryst. Solids* **2019**, *526*, 119726. [CrossRef]
90. Li, L.; Wang, F.; Liao, Q.; Wang, Y.; Zhu, H.; Zhu, Y. Synthesis of phosphate-based glass-ceramic wasteforms by a melt-quenching process: The formation process. *J. Nucl. Mater.* **2020**, *528*, 151854. [CrossRef]
91. Liang, X.F.; Lai, Y.; Yin, G.F.; Yang, S.Y. Effect of CeO_2 doped on the structure of phosphate calcium glass. *Chin. J. Inorg. Chem.* **2011**, *27*, 35–39.
92. Wang, F.; Li, L.; Zhu, H.; Liao, Q.; Zeng, J.; Wang, Y.; Wu, K.; Zhu, Y. Effects of heat treatment temperature and CeO_2 content on the phase composition, structure, and properties of monazite phosphate-based glass-ceramics. *J. Non-Cryst. Solids* **2022**, *588*, 121631. [CrossRef]
93. Stefanovsky, S.V.; Stefanovsky, O.I.; Myasoedov, B.F.; Vinikurov, S.E.; Danilov, S.S.; Nikonov, B.S.; Maslakov, K.I.; Teterind, Y.A. The phase composition, structure, and hydrolytic durability of sodium-aluminum-(iron)-phosphate glassy materials doped with lanthanum, cerium, europium, and gadolinium oxides. *J. Non Cryst. Solids* **2017**, *471*, 421–428. [CrossRef]

94. Stefanovskii, S.V.; Stefanovskaya, O.I.; Semenova, D.V.; Kadyko, M.I.; Danilov, S.S. Phase composition, structure, and hydrolytic stability of sodium-aluminum(iron) phosphate glass containing rare-earth oxides. *Glass Ceram.* **2018**, *75*, 89–94. [CrossRef]
95. Stefanovsky, S.V.; Stefanovsky, O.I.; Danilov, S.S.; Kadyko, M.I. Phosphate-based glasses and glass ceramics for immobilization of lanthanides and actinides. *Ceram. Int.* **2019**, *45*, 9331–9338. [CrossRef]
96. Wang, F.; Wang, Y.; Chen, J.; Liao, Q.; Zhu, H.; Zhou, J.; Qu, X.; Gong, Z.; Fu, X.; Zhu, Y. Effect of cerium oxide on phase composition, structure, thermal stability and aqueous durability of sodium-iron-boron-phosphate based glasses. *J. Nucl. Mater.* **2021**, *556*, 153199. [CrossRef]
97. Frolova, A.V.; Danilov, S.S.; Vinokurov, S.E. Corrosion behavior of some glasses immobilized with REE in simulated mineralized solutions. *Ceram. Int.* **2022**, *48*, 19644–19654. [CrossRef]
98. Matyunin, Y.I. Localization of components of liquid high-level wastes (REE, U, and Pu) in the phosphate and borosilicate glass-like materials. In *Extended Abstract of Candidate's (Chemistry) Dissertation*; VNIINM: Moscow, Russia, 2000. (In Russian)
99. Kong, L.; Wei, T.; Zhang, Y.; Karatchevtseva, I. Phase evolution and microstructure analysis of $CaZrTi_2O_7$ zirconolite in glass. *Ceram. Int.* **2018**, *44*, 6285–6292. [CrossRef]
100. Zhang, Y.; Zhang, Z.; Wei, T.; Kong, L.; Kim, Y.J.; Gregg, D.J. Pyrochlore glass-ceramics fabricated via both sintering and hot isostatic pressing for minor actinide immobilization. *J. Am. Ceram. Soc.* **2020**, *103*, 5470–5479. [CrossRef]
101. Maddrell, E.R.; Paterson, H.C.; May, S.E.; Burns, K.M. Phase evolution in zirconolite glass-ceramic wasteforms. *J. Nucl. Mater.* **2017**, *493*, 380–387. [CrossRef]
102. Maddrell, E.; Thornber, S.; Hyatt, N.C. The influence of glass composition on crystalline phase stability in glass-ceramic wasteforms. *J. Nucl. Mater.* **2015**, *456*, 461–466. [CrossRef]
103. NEA. *Management and Disposal of High-Level Radioactive Waste: Global Progress and Solutions*; NEA Rep. No. 7532; OECD/NEA Publishing: Paris, France, 2020; 45p.
104. Kochkin, B.; Malkovsky, V.; Yudintsev, S.; Petrov, V.; Ojovan, M. Problems and perspectives of borehole disposal of radioactive waste. *Prog. Nucl. Energy* **2021**, *139*, 103867. [CrossRef]
105. Deep Isolation Aiming for Disposal Site within Decade. World Nuclear News. 5 September 2022. Available online: https://world-nuclear-news.org/Articles/Deep-Isolation-aims-for-disposal-site-within-decad (accessed on 13 October 2023).
106. Ringwood, A. Disposal of high-level nuclear wastes: A geological perspective. *Mineral. Mag.* **1985**, *49*, 159–176. [CrossRef]
107. Brady, P.V.; Freeze, G.A.; Kuhlman, K.L.; Hardin, E.L.; Sassani, D.C.; MacKinnon, R.J. Deep borehole disposal of nuclear waste: US perspective. In *Geological Repository Systems for Safe Disposal of Spent Nuclear Fuels and Radioactive Waste*, 2nd ed.; Apted, M., Ahn, J., Eds.; Woodhead Publishing Series in Energy: Sawston, UK, 2017; Chapter 4; pp. 89–112.
108. Tsebakovskaya, N.S.; Barinov, A.S. Foreign news on spent nuclear fuel and radioactive waste. *Radioact. Waste* **2023**, *3*, 126–131. (In Russian)
109. Technical Evaluation of the, U.S. *Department of Energy Deep Borehole Disposal Research and Development Program: A Report to the U.S. Congress and the Secretary of Energy*; United States Nuclear Waste Technical Review Board: Arlington, VA, USA, 2016; 72p.
110. Kochkin, B.T.; Bogatov, S.A. Borehole rw disposal concept and prospects of its implementation in Russia. *Radioact. Waste* **2022**, *2*, 85–99. (In Russian) [CrossRef]
111. Freeze, G.; Phalen, J.; Mallants, D.; Sassani, D. Progress toward a deep borehole field demonstration. In Proceedings of the International High Level Radioactive Waste Management Conference (IHLRWM 2022), Phoenix, AZ, USA, 13–17 November 2022; 2023; pp. 1002–1006. [CrossRef]
112. Yudintsev, S.V. Isolation of separated waste of nuclear industry. *Radiochemistry* **2021**, *63*, 527–555. [CrossRef]
113. Yudintsev, S.V.; Nikolskii, M.S.; Nikonov, B.S.; Malkovskii, V.I. Matrices for isolation of actinide wastes in a deep well repository. *Dokl. Earth Sci.* **2018**, *480*, 631–636. [CrossRef]
114. Yudintsev, S.V.; Malkovsky, V.I.; Nikolsky, M.S.; Nikonov, B.S. Interaction of actinide matrices with brine. *Dokl. Earth Sci.* **2019**, *485*, 303–307. [CrossRef]
115. Malkovsky, V.; Yudintsev, S.; Ojovan, M. Forecast of ^{241}Am migration from a system of deep horizontal boreholes. *Sustainability* **2023**, *15*, 15134. [CrossRef]
116. Jantzen, C.M. Development of glass matrices for high level radioactive waste. In *Handbook of Advanced Radioactive Waste Conditioning Technologies*; Ojovan, M.I., Ed.; Woodhead Publishing Limited: Cambridge, UK, 2011; pp. 230–292.
117. Kim, C.-W.; Lee, B.G. Feasibility study on vitrification for rare earth wastes of pyrogreen process. *J. Korean Radioact. Waste Soc.* **2013**, *11*, 1–9. [CrossRef]
118. Kim, M.; Hong, K.-S.; Lee, J.; Byeon, M.; Jeong, Y.; Kim, J.H.; Um, W.; Kim, H.G. Evaluating thermal stability of rare-earth containing wasteforms at extraordinary nuclear disposal conditions. *Nucl. Eng. Technol.* **2021**, *53*, 2576–2581. [CrossRef]
119. Tong, Q.; Huo, J.; Zhang, X.; Cui, Z.; Zhu, Y. Study on structure and properties of La_2O_3-doped basaltic glasses for immobilizing simulated lanthanides. *Materials.* **2021**, *14*, 4709. [CrossRef] [PubMed]
120. Gibb, F.G.F.; Beswick, A.J. A deep borehole disposal solution for the UK's high-level radioactive waste. *Energy* **2021**, *175*, 11–29. [CrossRef]
121. Chapman, N.A. Who might be interested in a deep borehole disposal facility for their radioactive waste. *Energies* **2019**, *12*, 1542. [CrossRef]
122. Ewing, R.C.; Weber, W.J.; Lian, J. Nuclear waste disposal—Pyrochlore ($A_2B_2O_7$): Nuclear wasteform for the immobilization of plutonium and "minor" actinides. *J. Appl. Phys.* **2004**, *95*, 5949–5971. [CrossRef]

123. McMaster, S.A.; Ram, R.; Faris, N.; Pownceby, M.I. Radionuclide disposal using the pyrochlore supergroup of minerals as a host matrix-A review. *J. Hazard. Mater.* **2018**, *360*, 257–269. [CrossRef]
124. Blackburn, L.R.; Bailey, D.J.; Sun, S.-K.; Gardner, L.J.; Stennett, M.C.; Corkhill, C.L.; Hyatt, N.C. Review of zirconolite crystal chemistry and aqueous durability. *Adv. Appl. Ceram.* **2021**, *120*, 69–83. [CrossRef]
125. Wang, Y.; Jing, C.; Ding, Z.-Y.; Zhang, Y.-Z.; Wei, T.; Ouyang, J.-H.; Liu, Z.-G.; Wang, Y.-J.; Wang, Y.-M. The structure, property, and ion irradiation effects of pyrochlores: A comprehensive review. *Crystals* **2023**, *13*, 143. [CrossRef]
126. Jantzen, C.M.; Ojovan, M.I. On selection of matrix (wasteform) material for higher activity nuclear waste immobilisation (Review). *Russ. J. Inorg. Chem.* **2019**, *64*, 1611–1624. [CrossRef]
127. Logan, S.E. Deep self-burial of radioactive wastes by rock-melting capsules. *Nucl. Technol.* **1974**, *21*, 111–124. [CrossRef]
128. Efankin, V.G.; Kashcheev, V.A.; Poluektov, P.P. Laboratory modelling of self-disposal of radioactive wastes. *At. Energy* **1994**, *76*, 161–164. [CrossRef]
129. Gibb, F.G.F. High-temperature, very deep, geological disposal: A safer alternative for high-level radioactive waste? *Waste Manag.* **1999**, *19*, 207–211. [CrossRef]
130. Kosachevskiy, L.Y.; Sui, L.S. On the 'self-burial' of radioactive wastes. *J. Tech. Phys.* **1999**, *69*, 123–127. [CrossRef]
131. Stevenson, D.J. Mission to Earth's core—A modest proposal. *Nature* **2003**, *423*, 239–240. [CrossRef]
132. Ojovan, M.I.; Gibb, F.G.F.; Poluektov, P.P. Probing of the interior layers of the Earth with self-sinking capsules. *At. Energy* **2005**, *99*, 556–562.
133. Ojovan, M.I.; Gibb, F.G.F. Exploring the Earth's crust and mantle using self-descending, radiation-heated, probes and acoustic emission monitoring. In *Nuclear Waste Research: Siting, Technology and Treatment*; Lattefer, P.A., Ed.; Nova Science Publishers: New York, NY, USA, 2008; Chapter 7; pp. 207–220.
134. Spasova, L.M.; Ojovan, M.I.; Gibb, F.G.F. Acoustic emission on melting/solidification of natural granite simulating very deep waste disposal. *Nucl. Eng. Des.* **2012**, *248*, 329–339. [CrossRef]
135. Ojovan, M.I.; Poluektov, P.P.; Kashcheev, V.A. Self-disposal option for highly-radioactive waste reconsidered. *Mater. Res. Soc. Symp. Proc.* **2012**, *1475*, 429–434. [CrossRef]
136. Ojovan, M.I.; Poluektov, P.P.; Kascheev, V.A. The self-disposal option. *Nucl. Eng. Int.* **2012**, *57*, 28–29.
137. Gibb, F.G.F.; Taylor, K.J.; Burakov, B.E. The 'granite encapsulation' route to the safe disposal of Pu and other actinides. *J. Nucl. Mater.* **2008**, *374*, 364–369. [CrossRef]
138. Gibb, F.G.F. A new scheme for the very deep geological disposal of high-level radioactive waste. *J. Geol. Soc.* **2000**, *157*, 27–36. [CrossRef]
139. Chen, W.; Hao, J.; Chen, Z. A study of self-burial of a radioactive waste container by deep rock melting. *Sci. Technol. Nucl. Install.* **2013**, *2013*, 184757. [CrossRef]
140. Arutunyan, R.; Bolshov, L.; Shvedov, A. A new approach to radioactive waste self-burial using high penetrating radiation. *J. Nucl. Sci. Technol.* **2018**, *55*, 971–978. [CrossRef]
141. Byalko, A.V. *Nuclear Waste Disposal: Geophysical Safety*; CRC Press: Boca Raton, FL, USA, 1994; 281p.
142. Vityazev, A.V.; Zetser, Y.I.; Monastyrsky, I.B. Method of Disposal of Radioactive Waste. Patent No. RU 95110471, 20 June 1997. (In Russian).
143. Vityazev, A.V.; Zetser, Y.I.; Monastyrsky, I.B.; Khavroshkin, O.B. Method of Disposal of Radioactive Waste. Patent No. RU 2121723, 10 November 1998. (In Russian).
144. Arens, V.Z.; Vertman, A.A.; Kedrovsky, O.L.; Poluektov, P.P.; Polyakov, A.S.; Khavroshkin, O.B. Method of Disposal of Spent Nuclear Fuel. Patent No. RU 2127003, 27 February 1999. (In Russian).
145. Yang, P.; Wang, Y.; Rodriguez, M.A.; Brady, P.V. Rock-welding materials development for deep borehole nuclear waste disposal. *Mater. Chem. Phys.* **2019**, *221*, 178–187. [CrossRef]
146. Asuvathraman, R.; Joseph, K.; Madhavan, R.R.; Sudha, R.; Prabhu, R.K.; Govindan Kutty, K.V. A versatile monazite–IPG glass–ceramic wasteform with simulated HLW: Synthesis and characterization. *J. Eur. Ceram. Soc.* **2015**, *35*, 4233–4239. [CrossRef]
147. Ojovan, M.I. Challenges in the long-term behaviour of highly radioactive materials. *Sustainability* **2022**, *14*, 2445. [CrossRef]
148. Ojovan, M.I. The flow of glasses and glass–liquid transition under electron irradiation. *Int. J. Mol. Sci.* **2023**, *24*, 12120. [CrossRef]
149. Deng, Y.; Liao, Q.; Wang, F.; Zhu, H. Synthesis and characterization of cerium containing iron phosphate-based glass-ceramics. *J. Nucl. Mater.* **2018**, *499*, 410–418. [CrossRef]
150. Wang, F.; Wang, Y.; Liao, Q.; Zhang, J.; Zhao, W.; Yuan, Y.; Zhu, H.; Li, L.; Zhu, Y. Immobilization of a simulated HLW in phosphate-based glasses/glass-ceramics by melt-quenching process. *J. Non-Cryst. Solids* **2020**, *545*, 120246. [CrossRef]
151. Bailey, D.J.; Gardner, L.J.; Harrison, M.T.; McKendrick, D.; Hyatt, N.C. Development of monazite glass-ceramic wasteforms for the immobilisation of pyroprocessing wastes. *MRS Adv.* **2022**, *7*, 81–85. [CrossRef]
152. *GOST R50926-96*; Solidified High-Level Waste. General Technical Requirements. IPC Standards Publishing House: Bannockburn, IL, USA, 1996. (In Russian)
153. Criteria for the acceptability of radioactive waste for disposal. Federal Service for Environmental Protection, technological and nuclear supervision. *Nucl. Radiat. Saf.* **2015**, *3*, 59–82. (In Russian). Available online: https://docs.secnrs.ru/documents/nps/%D0%9D%D0%9F-093-14/%D0%9D%D0%9F-093-14.pdf (accessed on 3 December 2023).

154. *Collection, Processing, Storage and Conditioning of Liquid Radioactive Waste. Safety Requirements. Federal Norms and Rules in the Field of Atomic Energy Use*; Federal Service for Environmental Protection, Technological and Nuclear Supervision: Moscow, Russia, 2021; 21p. (In Russian)
155. Gin, S.; Abdelouas, A.; Criscenti, L.J.; Ebert, W.L.; Ferrand, K.; Geisler, T.; Harrison, M.T.; Inagaki, Y.; Mitsui, S.; Mueller, K.T.; et al. An international initiative on long-term behavior of high-level nuclear waste glass. *Mater. Today* **2013**, *16*, 243–248. [CrossRef]
156. Remizov, M.B.; Kozlov, P.V.; Logunov, M.V.; Koltyshev, V.K.; Korchenkin, K.K. Conceptual and technical solutions for the creation of vitrification units for current and accumulated liquid HLW at PA Mayak. *Issues Radiat. Saf.* **2014**, *3*, 17–25. (In Russian)
157. Vernaz, E.; Bruezière, J. History of nuclear waste glass in France. *Procedia Mater. Sci.* **2014**, *7*, 3–9. [CrossRef]
158. Harrison, M.T. Vitrification of high level waste in the UK. *Procedia Mater. Sci.* **2014**, *7*, 10–15. [CrossRef]